DuneFront

Deliverable 12.4

December 2025

DuneFront

Validation of numerical models XBeach-SB, XBeach-NH, and SWASH

Deliverable 12.4 – D12.4

Deliverable information

Title	Validation of numerical models XBeach-SB, XBeach-NH, and SWASH
Deliverable number	D12.4
WP number	12
Author(s)	Cem Sevindik, Marion Tissier, Bas Hofland
Lead beneficiary	TU Delft
Contributors	Cem Sevindik, Marion Tissier, Bas Hofland, Afshar Adeli, Vincent Gruwez
Type	Report
Dissemination level	Public
How to cite	Sevindik et al. (2026) Validation of numerical models XBeach-SB, XBeach-NH, and SWASH. DuneFront deliverable D12.4.
Copyright license*	© Authors and DuneFront consortium, 2024-2027. *This work is openly licensed via* CC-BY-4.0 , see https://creativecommons.org/licenses/by/4.0/

Versioning and contribution history

Version	Date	Authors (Institution)	Notes
Version 0.1	12 January 2026	TU Delft	Draft
Version 1.0			Final version approved by all Beneficiaries

Funded by the European Union. Views and opinions expressed are however those of the author(s) only and do not necessarily reflect those of the European Union. Neither the European Union nor the granting authority can be held responsible for them.

Funded by the European Union

DuneFront

Cover page

This report is the fourth deliverable of Work Package 12 (WP12 – D12.4 Validation of numerical models XBeach-SB, XBeach-NH, and SWASH) in the DuneFront project. DuneFront focuses on better understanding dune-dike hybrid Nature-based Solutions (DD-Hybrid NbS) to create sustainable, inclusive, and aesthetic coastal management infrastructure. These innovative solutions aim to integrate biodiversity while addressing significant socio-economic challenges along Europe's densely populated coasts.

The primary objective of Work Package (WP) 12 is to evaluate the coastal protection functioning of DD-Hybrid NbS during extreme storms. This requires gaining new insights into the physical processes specific to storm-wave interactions with DD-Hybrid NbS, such as dune erosion in the presence of a hard structure, the effect of the eroding dune on wave transformation, dike loading, wave overtopping, and wave impacts, but also dune strengthening by vegetation. To obtain this currently unavailable data on the functioning of DD-Hybrid NbS under extreme storm conditions, dedicated physical experiments are conducted on a selection of DuneFront demonstrators. The physical modelling data will be used to validate and improve the process-based numerical models and subsequently expand the physical model dataset for a wider range of conditions and geometries of the DD-Hybrid NbS.

The present report describes the hydrodynamic validation of numerical tools XBeach-SB, XBeach-NH, and SWASH using the dataset from the first DuneFront laboratory experiments (D12.1). In this deliverable (D12.4), TU Delft has modelled numerically a selection of 11 irregular wave sets from the first experimental campaign, in close collaboration with UGent-E. The primary objective of this task is to validate the aforementioned numerical models using the collected experimental data set, and determine which of these models (or a combination thereof) is the most accurate for modeling the hydrodynamic processes occurring when waves interact with DD–Hybrid NbS. In this validation study, several parameters, which include the mean water depth, incident and total significant wave heights for both sea-swell and infragravity frequency bands, and mean wave overtopping discharge, were considered.

In the present report, the numerical tools are briefly introduced in Section 2. Then, in Section 3, the validation procedure and data processing methodology are presented. In Sections 4 and 5, the results, along with comparisons and discussions, are presented, respectively. Finally, the present report ends with a conclusion in Section 6. In the Appendix, the results from all considered cases are presented.

DuneFront

Table of Contents

Notation

Parameter	Explanation
γ	Peak enhancement factor
H_{m0}	(Spectral) significant wave height (m)
$H_{m0,deep}$	Deep water (spectral) significant wave height (m)
$H_{m0,IG}$	Offshore significant wave height for free infragravity waves (m)
$H_{m0,,ss}$	Offshore significant wave height for sea-swell waves (m)
$H_{m0,IG,total}$	Total significant wave height for infragravity waves (m)
$H_{m0,IG,incident}$	Incident significant wave height for infragravity waves (m)
$H_{m0,SS,total}$	Total significant wave height for sea-swell waves (m)
$H_{m0,SS,incident}$	Incident significant wave height for sea-swell waves (m)
H_{exp}	Significant wave height measured in the experiments
H_{num}	Significant wave height measured in the simulations
H_{SS}	Total significant wave height (m)
H_{rms}	Root mean square wave height (m)
h	Water depth (m)
$h_{o,corrected}$	Corrected offshore water depth (m)
h_{toe}	Depth at toe of the dike after dune erosion (m)
k	Wave number (related to wave length)
n	Bed friction coefficient
T_p	Peak wave period (s)

List of abbreviations

Abbreviation	Explanation
BC	Base Case
BE	Belgium
DD	Dune-Dike
DD-Hybrid	Dune-Dike Hybrid
EMF	Electromagnetic Flow meter
FIR	Finite impulse response
IG	Infragravity waves
IR	Irregular
JONSWAP	Joint North Sea Wave Project
K	Katwijk
LED-PIV	Light Emitting Diode Particle Image Velocimetry
MATLAB	Matrix Laboratory
MIC	Mic Ultrasonic Sensor
NbS	Nature-based Solution
NL	The Netherlands
SS	Sea-swell waves
SWASH	Simulating Waves till Shore
SWL	Still Water Level
R	Raversijde
WG	Wave Gauge
WP	Work Package
XB-NH	XBeach Non-hydrostatic mode
XB-SB	XBeach Surfbeat mode

1. Introduction

1.1 General Background

The primary objective of the DuneFront project is to optimize dune-dike hybrid Nature-based Solutions (DD-Hybrid NbS) as a new generation of sustainable, nature-inclusive coastal protection. Such coastal protection measures, that combine a hard safety line (dike) and biodiverse and resilient dune systems, have the potential to adapt to sea-level rise provided that the physical and biological conditions are met. In this context, a key challenge of DuneFront is to identify the biological, physical, and socio-economic boundary conditions and their interactions to enhance the protection provided by these hybrid approaches. The DuneFront concept is summarized in Figure 1.

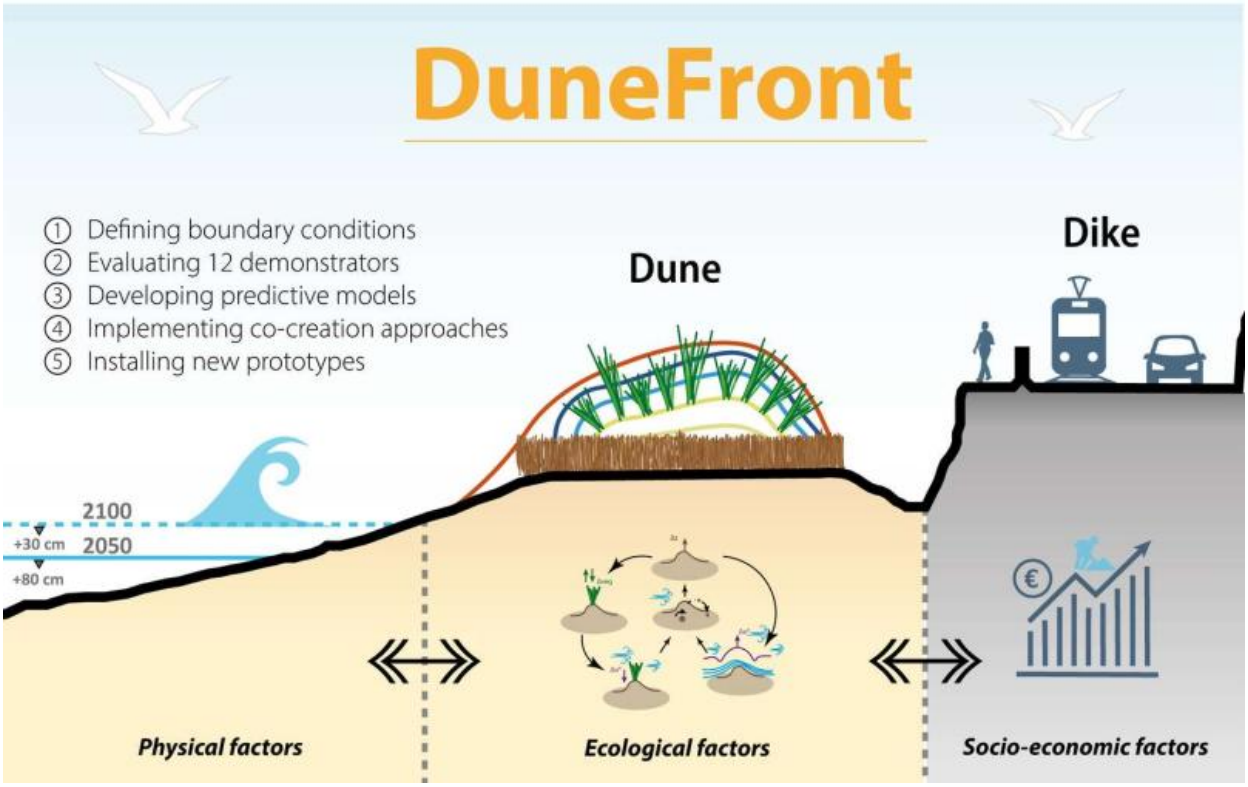

Figure 1 - DuneFront concept in one graphical abstract

1.2 Overview of Work Package 12

1.2.1 Work Package description

The primary objective of Work Package (WP) 12 is to evaluate the coastal protection functioning of DD-hybrid NbS during extreme storms. This requires gaining new insights into the physical processes specific to storm wave interactions with DD-hybrid NbS, such as dune erosion in the presence of a hard structure, the effect of the eroding dune on dike loading, wave overtopping, and wave impacts, but also dune strengthening by vegetation. To obtain

those, currently unavailable data on the functioning of DD-Hybrid NbS under extreme storm conditions will be collected using dedicated physical experiments of a selection of the DuneFront demonstrators, using the input from WP7. These so-called Physical Twins will also be used to communicate with stakeholders (WP17). The physical modeling data will be used to validate and improve the process-based numerical models and subsequently expand the physical model dataset for a wider range of conditions and geometries of the DD-Hybrid NbS. Ultimately, this will be used to demonstrate the efficiency of the DD-Hybrid NbS coastal protection system as an adaptive defense against climate change impacts.

1.2.2 Work Package sub-tasks and deliverables

WP12 consists of 5 tasks listed below, each of them associated with a deliverable:

Task 12.1. Physical modeling of the Dutch Demonstrator(s), focus: wave-dike interactions (Deliverable D12.1)

Task 12.2. Physical modeling of the German Demonstrator(s), focus: vegetation influence on dune erosion (Deliverable D12.2, March 2026)

Task 12.3. Physical modeling of the Belgian Demonstrator(s), focus: dune-dike interactions (Deliverable D12.3, September 2026)

Task 12.4. Validation of the numerical models XBeach-SB, XBeach-NH, and SWASH using the experimental data (Deliverable D12.4, December 2025)

Task 12.5. Demonstration of the DD-hybrid NbS coastal protection efficiency using the validated models (Deliverable D12.5, June 2027)

1.3 Aims of D12.4

Within the scope of D12.4 (this report), TU Delft has validated the numerical tools XBeach-SB, XBeach-NH, and SWASH with the physical model data within the scope of D12.1 in close collaboration with UGENT-E and FH. This study has been carried out to determine which of these models (or a combination thereof) is the most accurate for modelling hydrodynamic processes occurring when waves interact with DD-Hybrid NbS. The validated numerical modelling methodology will be used in WP13.

1.4 Outline of this report

This report is structured as follows: Section 2 gives brief information about the numerical tools XBeach and SWASH, and then, Section 3 describes the methodology followed for the validation process. Later, in Sections 4 and 5, results from the cases and related discussions are given. These are followed by Section 6, which presents the conclusions and recommendations. Finally, the report ends with an Appendix including the results (such as mean water depth and significant wave height evolution along the domain, and percent errors

on significant wave heights observed from numerical simulations based on the experimental data) from all studied cases.

2. Numerical Tools

2.1 General Background

In the scope of D12.1, two numerical tools were used to complete the deliverable. These are XBeach and SWASH. For this work, two options of XBeach are considered, which are Surfbeat (XBeach-SB) and Non-hydrostatic (XBeach-NH) models. In this section of the report, these two numerical tools and two modes for XBeach are briefly introduced.

2.2 XBeach

XBeach (Roelvink et al., 2009) is a two-dimensional, open-source numerical model originally developed to simulate hydrodynamic and morphodynamic processes and their impacts on sandy coasts, with a domain size of kilometers and a timescale of storms. Since then, the model has been applied to other types of coasts and purposes.

The model includes the hydrodynamic processes of short-wave transformation (refraction, shoaling, and breaking), long-wave (infragravity wave) transformation (generation, propagation, and dissipation), wave-induced setup and unsteady currents, as well as overwash and inundation. The morphodynamic processes include bed load and suspended sediment transport, dune face avalanching, bed update, and breaching. The effects of vegetation and hard structures have been included. The model has been validated with a series of analytical, laboratory, and field test cases using a standard set of parameter settings (XBeach Team, 2023).

2.2.1 Surfbeat Mode (XB-SB)

In the Surfbeat mode, the short-wave motion is solved using the wave action equation, which is a time-dependent forcing of the HISWA equations (Holthuijsen et al., 1989). This equation solves the variation of the short-waves envelope (wave height) on the scale of wave groups. Hence, the separate short waves are not resolved by the model. It employs a dissipation model for use with wave groups (Daly et al., 2012, Roelvink, 1993) and a roller model (Nairn et al., 1990, Stive and De Vriend, 1994, Svendsen, 1984) to represent momentum stored at the surface after breaking. These variations, through radiation stress gradients (Longuet-Higgins and Stewart, 1962; 1964), exert a force on the water column and drive longer-period waves (infragravity waves) and unsteady currents, which are solved by the nonlinear shallow water equations (Phillips, 1977). Thus, wave-driven currents (longshore current, rip currents, and undertow), and wind-driven currents (stationary and uniform) for local wind set-up, long (infragravity) waves, and runup and rundown of these long waves (swash) are resolved by the model.

In the Surfbeat mode, short waves run-up is not resolved. It is therefore valid on dissipative beaches, where the short waves are mostly dissipated by the time they are near the shoreline. On intermediate beaches during extreme events, the swash motions are still predominantly in the infragravity band, and so is the runup (XBeach Team, 2023).

2.2.2 Non-Hydrostatic Mode (XB-NH)

In Non-hydrostatic mode (XB-NH), XBeach computes the depth-averaged flow induced by waves and currents using the nonlinear shallow-water equations augmented with a non-hydrostatic pressure term. The depth-averaged normalized dynamic pressure (q) is formulated like the one-layer configuration of the SWASH model (Zijlema et al., 2011), where the dynamic pressure is assumed to be zero at the free surface and to vary linearly over the water depth, such that the depth-averaged value is obtained from the mean of the surface and bed pressures. This formulation introduces dispersive effects into the long-wave equations, enabling the model to resolve short-wave motions in shallow to intermediate water depths. No explicit limitation is defined in terms of the nondimensional parameter kh, where k is the wave number (related to wavelength), and h is the local water depth, representing the relative water depth regime. The single-layer NH formulation is most reliable for $kh \lesssim 1–2$. To improve the dispersive behaviour, the (reduced) two-layer non-hydrostatic option was implemented in the XB-NH simulations (de Ridder et al., 2021; XBeach Team, 2023), in which the water column is divided into two depth-averaged layers with independent velocities and non-hydrostatic pressures, extending the practical applicability to approximately $kh \lesssim 2–3$. Wave breaking is implemented by disabling the non-hydrostatic pressure term when waves exceed a certain steepness, after which the bore-like breaking implicit in the momentum-conserving shallow water equations takes over.

In case the non-hydrostatic mode is used, the short-wave action balance is no longer required. This saves computation time. However, in the wave-resolving mode, much higher spatial resolution and associated smaller time steps are needed to make this mode much more computationally expensive than the Surfbeat mode. The main advantages of the non-hydrostatic mode are that the incident-band (short-wave) runup and overwashing are included, which is especially important on steep slopes. Another advantage is that the model resolves wave asymmetry and skewness, eliminating the need for approximate local models or empirical formulations for these terms. Finally, in cases where diffraction is a dominant process, wave-resolving modeling is needed as it is neglected in the short-wave averaged mode. Although sandy morphology can be simulated using the wave-resolving mode, it has not been extensively validated, and changes in the sediment transport formulations will likely be implemented in the near future (XBeach Team, 2023). Therefore, XBeach-SurfBeat remains at this stage the most extensively validated XBeach mode for dune erosion modelling.

2.3 SWASH

SWASH is a general-purpose numerical tool for simulating non-hydrostatic, free-surface, rotational flows and transport phenomena in one, two, or three dimensions. The governing equations are the nonlinear shallow water equations, including a non-hydrostatic pressure correction. It also includes some scalar transport equations. It provides a general basis for simulating (The SWASH Team, 2024):

- wave transformation in both surf and swash zones due to nonlinear wave-wave interactions, interaction of waves with currents, interaction of waves with structures, wave damping due to vegetation, and wave breaking as well as runup at the shoreline,
- complex changes to rapidly varied flows typically found in coastal flooding resulting from, e.g., dike breaks, tsunamis, and flood waves,
- density-driven flows in coastal seas, estuaries, lakes, and rivers, and
- large-scale ocean circulation, tides, and storm surges.

The model is referred to as a wave-flow model and is essentially applicable in the coastal regions up to the shore. This has prompted the acronym SWASH for the associated code, standing for **S**imulating **WA**ves till **SH**ore. The basic philosophy of the SWASH code is to provide an efficient and robust model that allows its application to a wide range of time and space scales of surface waves and shallow water flows in complex environments. As a result, SWASH allows for the entire modelling process to be carried out in any area of interest. This includes small-scale coastal applications, like waves approaching a beach, wave penetration in a harbour, flood waves in a river, oscillatory flow through canopies, salt intrusion in an estuary, and large-scale ocean, shelf, and coastal systems driven by Coriolis and meteorological forces to simulate tidal waves and storm surge floods (The SWASH Team, 2024).

3. Methodology

In the scope of this deliverable, experimental data gathered during the first experimental campaign of WP12 were used to validate XBeach and SWASH numerical tools. This section consists of three parts. The first part provides a summary of the experimental setup, which is explained in detail in D12.1 (Sevindik et al., 2025). The second part summarizes the methodology followed for the numerical simulations. And finally, this chapter ends with the post-processing part explaining key steps taken for analyzing and comparing the physical model and numerical data.

3.1 Experimental Setup

The laboratory experiments were conducted in the wave flume of the Hydraulic Engineering Laboratory at Delft University of Technology, Delft, The Netherlands, from April to June 2025. The flume is 39 m long, 0.79 m wide, and 1 m high; it has glass windows along most of its length. The waves were generated with a piston-type wave maker with a 2 m stroke, and equipped with Active Reflection Compensation (ARC) to minimize reflections from the wave paddle.

Model setups were designed with an approximately **1/25 Froude-type length scale** compared to selected of the DuneFront demonstrators. In these experiments, two different DD-Hybrid NBs, namely the Raversijde (BE) dune-in-front-of-dike type hybrid structure and the Katwijk (NL) dike-in-dune type hybrid structure, were investigated under various hydraulic conditions. In the experiments, fully eroded profiles of these structures under extreme hydraulic loading were studied, and a reference case (Base Case) scenario was also considered. In this reference case, sand deposition resulting from theeroded dune part of the DD-Hybrid NbS was neglected. The fixed bed profiles were made of plywood material. Experiments were furthermore conducted in two phases, and in each phase, the three different bed configurations mentioned above, representing Base Case (BC), Raverijde (R), and Katwijk (K) were applied. These phases are described below, focusing on the wave conditions and instruments used for model validation in this deliverable.

In Phase 1 of the experiment, the three main bed profiles were successively considered, and a dike structure was installed shoreward of these profiles (see Figure 2). Water surface elevation along the domain was measured by 14 wave gauges (WGs), and flow velocity along the domain was measured by 9 electromagnetic flow meters (EMFs), water layer thickness on the crest was measured by 2 ultrasonic sensors (MIC), and wave overtopping was measured by 1 WG and MIC inside the wave overtopping box located at the back side of the dike part. These instruments sampled data at a frequency of 500 Hz. Two different water depths at the dike toe (h_{toe}= 5 cm and 10 cm, corresponding to 1.25 m and 2.5 m in prototype scale) were considered. For the Base Case configuration, both values (corresponding to 65.2 cm and 70.2 cm offshore water depths, respectively) were applied, but for the Raversijde and Katwijk configurations, only a 5 cm water depth at the dike toe (70.8 cm offshore water depth) was

considered. A drawing of the setup for Phase 1 is given in Figure 2 for the three profiles considered.

In Phase 2 of the experiment, the same bed profiles are considered, but now without the dike. Those cases are not used in the present validation study.

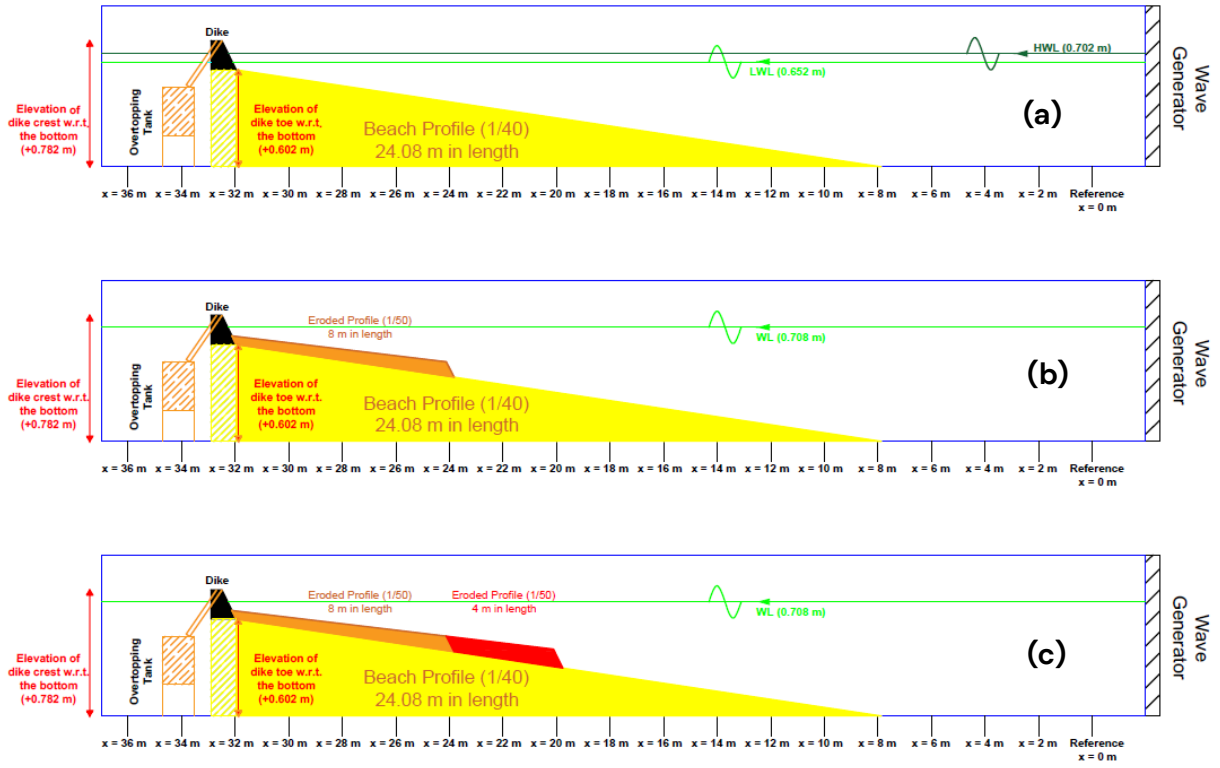

Figure 2 - Bed profiles for Phase 1 of the experiments with (a) the dike-only base case (BC), (b) the "Raversijde" (R) eroded profile, and (c) the "Katwijk" (K) eroded profile (horizontal and vertical scales differ).

During the physical modeling campaign, a total of 168 tests were carried out. 84 of those were carried out in Phase 1 (with the dike), and 84 were carried out in Phase 2 (after removing the dike). Out of the 84 wave sets in each phase, 39 were irregular wave sets. For the irregular wave sets, the signals were based on a JONSWAP spectrum with a peak enhancement factor γ of 3.3. Peak periods varied between 1.6 s and 2.8 s, while the significant wave height varied between 0.08 m and 0.16 m.

3.2 Numerical Simulations

As mentioned, the numerical tools XBeach (both Surfbeat and Non-hydrostatic modes) and SWASH were used for the validation study. The validation focuses on the irregular wave sets. For this, 11 irregular wave sets were selected: five sets from the Base Case configuration, and three wave sets from both the Raversijde and Katwijk configurations. This selection was made

to limit the number of calculations. Irregular sets were selected as they best represent reality and are therefore best suited to validate wave transformation and setup. Furthermore, the selected conditions cover the entire measurement range (max to min), all demonstrators, and the design conditions for the two demonstrators. The other types of experimental wave sets (bichromatic waves and irregular waves, including additional free IG waves) will be used in later detailed process studies.

The considered wave sets (including their significant wave heights (H_{m0}), peak wave periods (T_p), offshore water depth, and water depth at the toe) for each configuration are given below. The test IDs are also given.

For the Base Case configuration, the tests listed below were considered for validation.

- $\mathrm{H_{m0}} = 0.08\ \mathrm{m}, \mathrm{T_p} = 1.6\ \mathrm{s}, \text{and } 65.2\ \mathrm{cm}\ \text{water depth}, \mathrm{h_{toe}} = 5\ \mathrm{cm}$ (BC_652_IR_8_16)
- $\mathrm{H_{m0}} = 0.16\ \mathrm{m}, \mathrm{T_p} = 2.8\ \mathrm{s}, \text{and } 65.2\ \mathrm{cm}\ \text{water depth}, \mathrm{h_{toe}} = 5\ \mathrm{cm}$ (BC_652_IR_16_28)
- $\mathrm{H_{m0}} = 0.08\ \mathrm{m}, \mathrm{T_p} = 1.6\ \mathrm{s}, \text{and } 70.2\ \mathrm{cm}\ \text{water depth}, \mathrm{h_{toe}} = 10\ \mathrm{cm}$ (BC_702_IR_8_16)
- $\mathrm{H_{m0}} = 0.16\ \mathrm{m}, \mathrm{T_p} = 1.6\ \mathrm{s}, \text{and } 70.2\ \mathrm{cm}\ \text{water depth}, \mathrm{h_{toe}} = 10\ \mathrm{cm}$ (BC_702_IR_16_16)
- $\mathrm{H_{m0}} = 0.16\ \mathrm{m}, \mathrm{T_p} = 2.8\ \mathrm{s}, \text{and } 70.2\ \mathrm{cm}\ \text{water depth}, \mathrm{h_{toe}} = 10\ \mathrm{cm}$ (BC_702_IR_16_28)

For the Raversijde configuration, the tests listed below were considered for validation.

- $\mathrm{H_{m0}} = 0.08\ \mathrm{m}, \mathrm{T_p} = 1.6\ \mathrm{s}, \text{and } 70.8\ \mathrm{cm}\ \text{water depth}, \mathrm{h_{toe}} = 5\ \mathrm{cm}$ (R_708_IR_8_16)
- $\mathrm{H_{m0}} = 0.16\ \mathrm{m}, \mathrm{T_p} = 1.6\ \mathrm{s}, \text{and } 70.8\ \mathrm{cm}\ \text{water depth}, \mathrm{h_{toe}} = 5\ \mathrm{cm}$ (R_708_IR_16_16)
- $\mathrm{H_{m0}} = 0.16\ \mathrm{m}, \mathrm{T_p} = 2.8\ \mathrm{s}, \text{and } 70.8\ \mathrm{cm}\ \text{water depth}, \mathrm{h_{toe}} = 5\ \mathrm{cm}$ (R_708_IR_16_28)

For the Katwijk configuration, the tests listed below were considered for validation.

- $\mathrm{H_{m0}} = 0.08\ \mathrm{m}, \mathrm{T_p} = 1.6\ \mathrm{s}, \text{and } 70.8\ \mathrm{cm}\ \text{water depth}, \mathrm{h_{toe}} = 5\ \mathrm{cm}$ (K_708_IR_8_16)
- $\mathrm{H_{m0}} = 0.16\ \mathrm{m}, \mathrm{T_p} = 1.6\ \mathrm{s}, \text{and } 70.8\ \mathrm{cm}\ \text{water depth}, \mathrm{h_{toe}} = 5\ \mathrm{cm}$ (K_708_IR_16_16)
- $\mathrm{H_{m0}} = 0.16\ \mathrm{m}, \mathrm{T_p} = 2.8\ \mathrm{s}, \text{and } 70.8\ \mathrm{cm}\ \text{water depth}, \mathrm{h_{toe}} = 5\ \mathrm{cm}$ (K_708_IR_16_28)

Bed profiles of each configuration were mimicked in the simulations. In Figure 3, the numerical domains are presented for the three configurations.

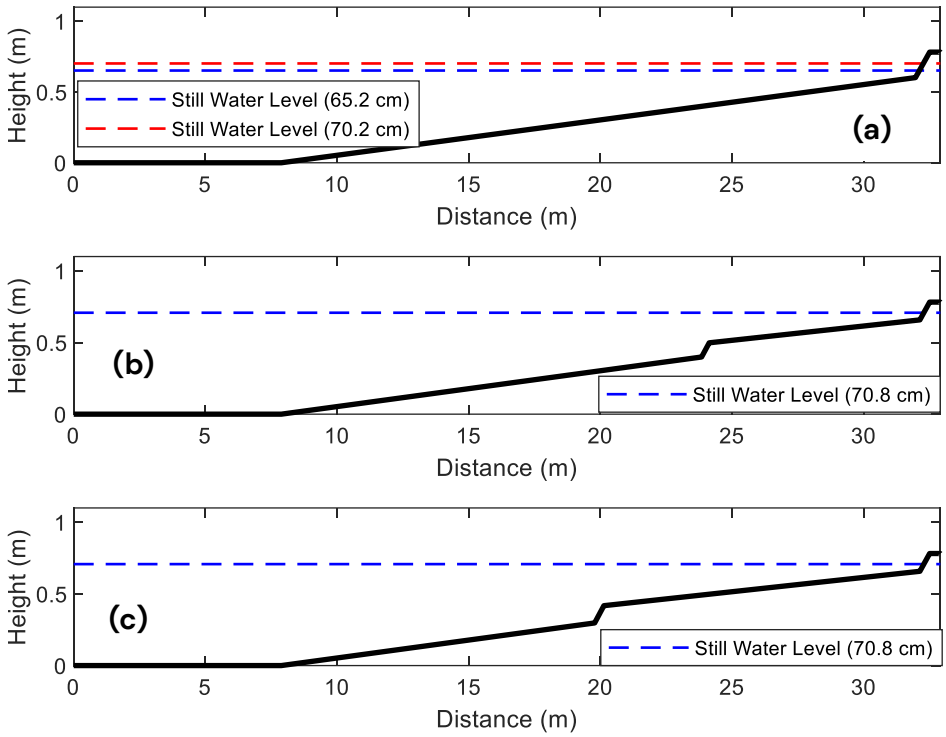

Figure 3 - A plot of the numerical domains for (a) Base Case, (b) Raversijde, and (c) Katwijk. Note that the back of the dike is not shown on the figure but included in the numerical domain. The still water levels for the selected test cases are also indicated.

All numerical simulations were carried out in 1D, and the applied signals were created based on a JONSWAP spectrum with a peak enhancement factor γ of 3.3 to mimic the laboratory forcing. In both numerical tools, a 1 cm grid size in the wave propagation direction (flume direction, x-direction) was used to achieve greater precision. For the boundary conditions of the numerical models, absorbing-generating (weekly reflecting) flow boundaries in 1D were applied on the inlet (offshore) and the outlet of the numerical domain. For the lateral flow boundaries, Neumann boundary conditions with a constant water level gradient were considered.

In the XB-SB and XB-NH simulations, outputs were collected at 153 distinct measurement points throughout the domain. To improve the dispersive behaviour, the (reduced) 2-layer non-hydrostatic option (XBeach Team, 2023; de Ridder et al., 2021) was implemented in XB-NH simulations. In this option, the pressure in the vertical is described by a hydrostatic pressure assumption in the bottom layer and a non-hydrostatic distribution in the upper layer. In SWASH simulations, a total of 741 measurement points were used for outputs, and the 2-layer option was also used in SWASH.

In all three numerical models and on all measurement points;

- Water surface elevation ($\eta, in\ m$)
- Depth-averaged velocity (u in $\mathrm{m/s}$, in both x and y directions)
- Discharge – Wave overtopping (q, in both x and y directions)
- Water depth (h, in m)

parameters were collected. In XB-SB and XB-NH simulations, a 50 Hz sampling frequency was applied to all parameters. This value was chosen as 25 Hz for SWASH simulations.

While carrying out the physical model study, an amount of water was lost because of the wave overtopping events, and this lost water was collected in the wave overtopping box located at the back side of the dike structure. Thus, the water level was not constant during the whole wave set in the physical modelling, and it decreased by a certain amount. This amount was not constant for all wave sets (changing between 2 and 6 mm in the whole wave flume) and depended not only on the offshore wave parameters (H_{m0} and T_p) but also the water level. Due to this situation, before starting the numerical simulations, the water level lost for each considered case was computed, determining the mean water depth at the first 5 WGs located in the offshore region of the flume. In the experiments, an additional two-minute measurement was taken before starting and after finishing the sets. The average values of the first and the last minutes of the water surface elevation data from those 5 WGs were taken. The difference between the average values was determined, and these values were reduced from the simulation water depth. This procedure was aimed at matching the water depths in numerical tools to the physical model. Below, reduction values of water depths and corrected offshore water depths for setup and overtopping ($h_{0,corrected}$) are given for each wave set.

For the Base Case configuration,

- BC_652_IR_8_16 ($2\ mm, h_{0,corrected} = 65.0\ cm$)
- BC_652_IR_16_28 ($2\ mm, h_{0,corrected} = 65.0\ cm$)
- BC_702_IR_8_16 ($4\ mm, h_{0,corrected} = 69.8\ cm$)
- BC_702_IR_16_16 ($5\ mm, h_{0,corrected} = 69.7\ cm$)
- BC_702_IR_16_28 ($6\ mm, h_{0,corrected} = 69.6\ cm$)

For the Raversijde configuration, the tests listed below were considered for validation.

- R_708_IR_8_16 ($2\ mm, h_{0,corrected} = 70.6\ cm$)
- R_708_IR_16_16 ($3\ mm, h_{0,corrected} = 70.5\ cm$)
- R_708_IR_16_28 ($4\ mm, h_{0,corrected} = 70.4\ cm$)

For the Katwijk configuration, the tests listed below were considered for validation.

- K_708_IR_8_16 ($3\ mm, h_{0,corrected} = 70.5\ cm$)
- K_708_IR_16_16 ($3\ mm, h_{0,corrected} = 70.5\ cm$)
- K_708_IR_16_28 ($3\ mm, h_{0,corrected} = 70.5\ cm$)

3.3 Post-processing

In the analysis part of the study, the mean water depth, total and incident significant wave heights for sea-swell (SS) and infragravity (IG) wave bands, and mean wave overtopping will be validated by comparing the experimental and numerical outcomes. Both the spatial development is qualitatively compared, and the values are quantitatively compared using error metrics. In this section, the methods used to analyze the numerical and experimental data are summarized.

Before calculating wave statistics and mean water levels, the surface elevation and velocity time series are cropped to ensure stationarity. In practice, the first 30 seconds of wave data are removed to remove spin-up effects, and the analysis is performed on the following record.

For the experimental data, the total mean water depths are calculated as the averages of the time series from the 14 WGs after calibration. For numerical data, the average values of the water surface elevation time series from 153 points in XB-SB and XB-NH, as well as from 741 points in SWASH, were used to compare the numerical and experimental data. Total mean water depth values were then compared at 14 points along the domain where the WGs were located in the experiments.

To decompose the incident and reflected time series from the total time series of the water surface elevation in the experimental dataset, water surface elevation and velocity measurements were used. A total of 9 EMFs were used in the experiments, and these were all placed collocated with a WG. Buckley's decomposition method (Buckley et al., 2015) was used for the experimental data, and since both water surface elevation and flow velocity in the direction of wave propagation are required, the incident time series in the experimental data could only be obtained for the 9 points where both the WG and EMF were present.

Unlike the experimental data, all the numerical output points could be used for decomposition since at all points velocity measurements were recorded, together with the water surface elevation, in the numerical simulation outputs. To decompose the time series gathered at all points in the numerical simulation outputs, an extension of the method of Guza et al. (1984) valid for intermediate water depths was used instead of Buckley et al. (2015). The reason behind it is that the velocity data in the experiments are point measurements of velocities at a certain elevation, but in the numerical data, the velocities were gathered as depth-averaged velocities.

After decomposing the incident and the reflected time series for the water surface elevation records, the following parameters were calculated from spectral analysis:

- Total significant wave height on IG wave band ($H_{m0,IG,total}$)
- Incident significant wave height on IG wave band ($H_{m0,IG,incident}$)

- Total significant wave height on SS wave band ($H_{m0,SS,total}$)
- Total significant wave height on SS wave band ($H_{m0,SS,incident}$)

In this analysis, IG and SS waves were separated by applying different frequency bands to them.

IG waves, also known as low-frequency waves, are surface ocean waves with lower frequencies than SS waves, in other words, long waves. Typical SS frequencies are between 0.04 and 1 Hz, whereas IG wave frequencies are generally defined as being between 0.004 and 0.04 Hz, in real life. We applied a 0.02-0.2 Hz band for IG waves and a 0.2-5 Hz band for SS waves by considering the 1/25 Froude length scale (and related 1/5 time scale) of the experimental setup. To remove the noise in the water surface elevation data, the frequency band of SS waves was narrowed to 0.2-2 Hz in the analysis part. The total water surface elevation time series was used to calculate $H_{m0,IG,total}$ and $H_{m0,SS,total}$, and the incident water surface elevation time series were used to calculate $H_{m0,IG,incident}$ and $H_{m0,SS,incident}$. Unlike XB-NH and SWASH, in XB-SB mode, a different approach was followed to determine $H_{m0,SS,total}$ and $H_{m0,SS,incident}$ parameters. Since the short-waves (SS waves) are solved as the variation of the short-waves envelope (wave height) on the scale of wave groups, the following equation was applied to determine these parameters from the outputs of XB-SB simulations.

$$H_{m0,SS,total} = \sqrt{{H_{ss}}^2 + \left(H_{rms} * \sqrt{2}\right)^2}$$

In the equation, H_{ss} refers to the total significant wave height on the SS wave band gathered from the water surface elevation in XB-SB (calculated by the nonlinear shallow water part of the model) and H_{rms} refers to the root mean square wave height calculated from the short-wave action balance, which was directly gathered as an output parameter. Here, another important point to mention is that the reflection process of short waves is not included in XB-SB. So, for the SS wave band in XB-SB, the total and incident significant wave height values in the SS wave band are assumed equal.

$$H_{m0.SS,total} = H_{m0,SS,incident}$$

For the mean wave overtopping analysis, the data gathered by the WG and MIC located in the wave overtopping box were used. Because of the noise in the gathered data, low-pass filters were applied to the data taken from these measurement devices to observe the mean wave overtopping value of each wave set. To the WG data, the low-pass filter of MATLAB was applied, with a 1 Hz low-pass frequency. For the MIC data, a 100th-order finite impulse response (FIR) type low-pass filter was used to denoise the signal with a 0.06 Hz cut-off frequency.

After the signal analysis, the total amount of overtopped water (in m^3) was calculated by multiplying the surface area of the overtopping box by the increase in water level. This value was divided by the duration of the wave set in seconds and the width of the overtopping

chute (15 cm) used to collect the overtopped water on the dike crest. So, the mean wave overtopping value was calculated in $m^3/s/m$ unit for both the WG and MIC. In the numerical data, discharge values (in m^2/s) on the seaward dike crest line were used for the mean wave overtopping calculations.

4. Results

In this part of the report, the results of the validation study are presented. This section consists of three parts, one part for each configuration, and additional results for this section are given in Appendix A, Appendix B, and Appendix C for Base Case, Raversijde, and Katwijk configurations, respectively.

4.1 Base Case configuration

In this part, the results for the Base Case (BC) configuration are presented. In the scope of the study, 5 different irregular wave cases were examined for this configuration by considering both toe water depths (h_{toe}), which are 5 cm and 10 cm (1.25 m and 2.5 m, respectively, in prototype scale). The names used for each case and studied h_{toe} values in these cases are given below.

- BC_652_IR_8_16 ($\boldsymbol{T01}$) - $h_{toe} = 5\ cm$
- BC_652_IR_16_28 ($\boldsymbol{T02}$) $h_{toe} = 5\ cm$
- BC_702_IR_8_16 ($\boldsymbol{T03}$) - $h_{toe} = 10\ cm$
- BC_702_IR_16_16 ($\boldsymbol{T04}$) - $h_{toe} = 10\ cm$
- BC_702_IR_16_28 ($\boldsymbol{T05}$) - $h_{toe} = 10\ cm$

In the figures given below (Figure 4 and Figure 5) the evolution of the mean water depth, and of the significant wave height for both IG and SS wave bands (for total and incident wave heights, respectively) of the irregular wave set T04 along the experimental and numerical domains is presented, as an example. The same graphs and percent errors for the significant wave heights for the other cases are presented in Appendix A.

For the mean water depth, the errors are not more than 1 % on any of the points. For significant wave height values, there are some mismatches, especially for the incident SS waves that are overestimated by the numerical models over the entire profile (Figure 5, second panel). The incident SS wave height is actually already slightly overestimated at the most offshore wave gauge. A similar behavior is observed for most test cases (see Appendix A for the cross-shore evolution of the wave height for all cases and the scatter plots in Figure 7). This indicates that, overall, the numerical predictions would improve by slightly adjusting the model input to match the observed offshore incident SS wave height, rather than imposing the target wave height (as defined at the laboratory) at the offshore boundary as done now. Preliminary test calculations, however, suggest that such an adjustment is not sufficient to solve the observed discrepancies in SS wave height in the nearshore.

The three numerical models predict a very similar cross-shore evolution of the SS and IG wave heights for most cases (e.g., Figure 4 and Figure 5). Only notable exceptions are cases T02 and T05, which are the most nonlinear cases in the validation study (the largest offshore wave height and period). For these specific cases, SWASH overestimates the IG wave height at the offshore boundary already (e.g., Figure 22 in Appendix A). This is somewhat surprising as the offshore boundary condition for the long waves in XB-NH and SWASH relies on the same approach (equilibrium bound long waves, Hasselmann (1962)) and should therefore result in similar amounts of incoming IG wave energy at the boundary. The reason for the observed discrepancy for these specific cases is unclear and should be further investigated in the future.

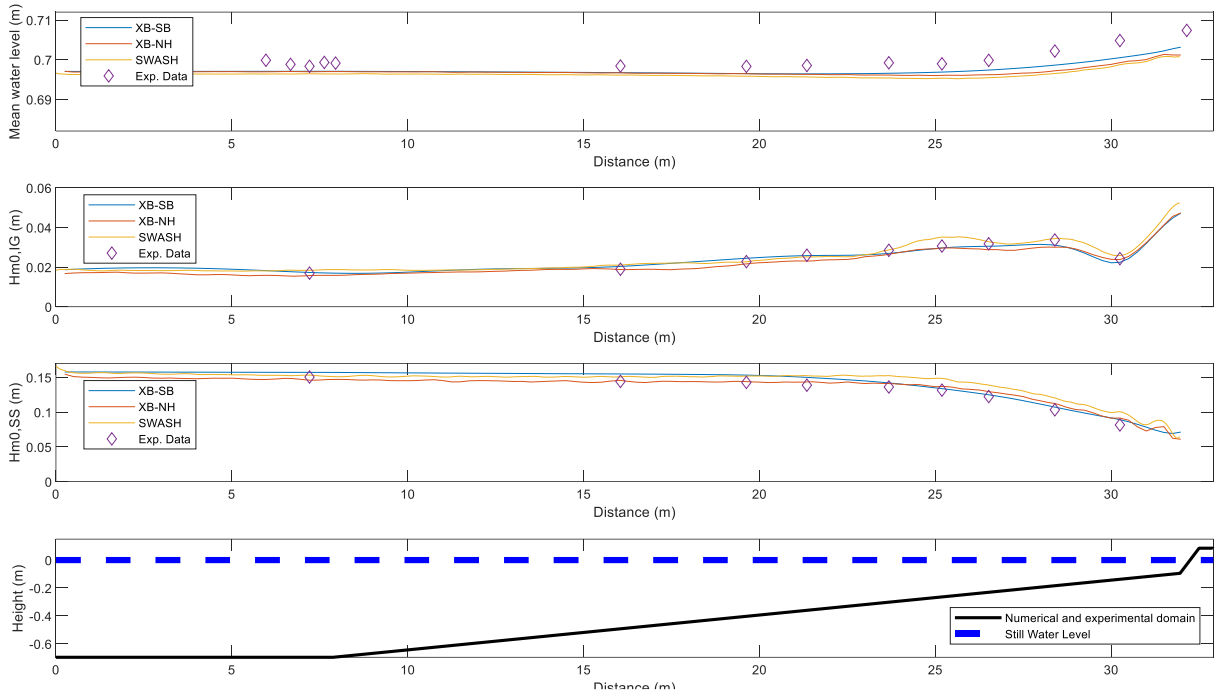

Figure 4 - Mean water depth (first panel) and total wave height for the infragravity (second panel) and sea-swell (third panel) waves along the domain for BC_702_IR_16_16 (T04) for the three numerical (colored lines) and for the data (diamonds).

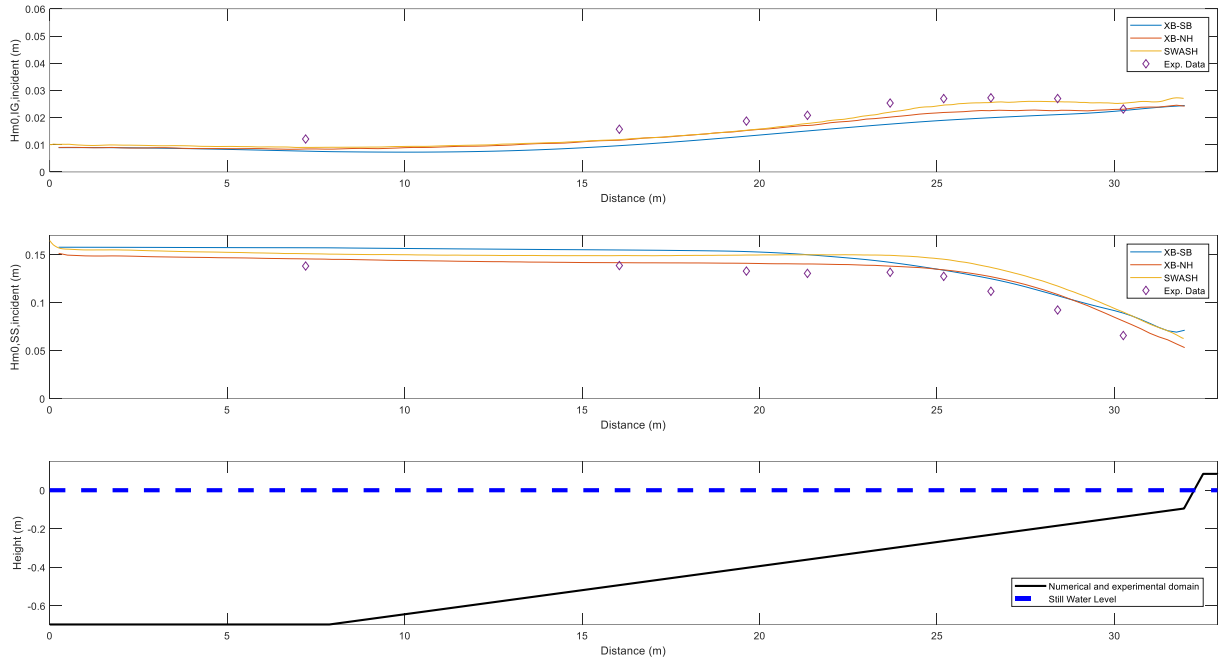

Figure 5 - Incident wave height for the infragravity (first panel) and sea-swell (second panel) waves along the domain for BC_702_IR_16_16 (T04) for the three numerical (colored lines) and for the data (diamonds).

Figure 6 and Figure 7 compare the total and incident IG and SS wave heights at nine different measurement locations for all wave sets considered for the Base Case configuration (T01, T02, T03, T04, and T05), including both water depths (65.2 cm and 70.2 cm).

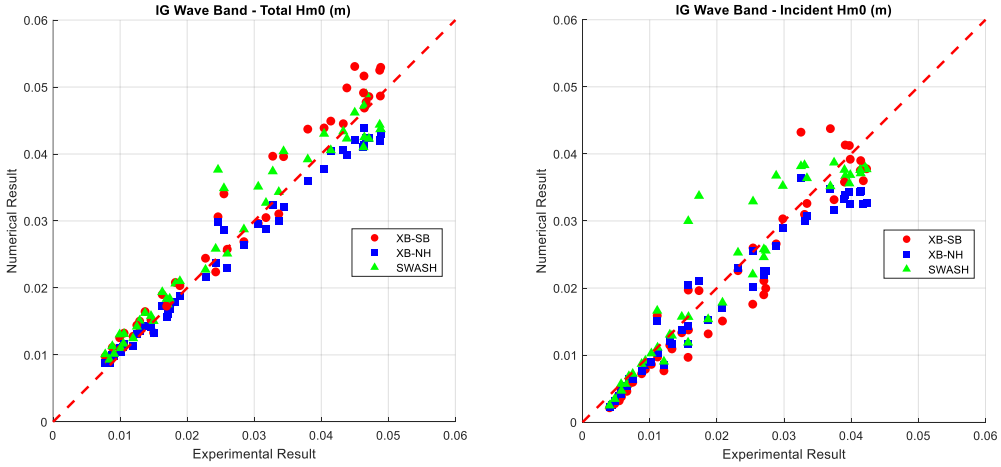

Figure 6 - Comparison of the numerical and experimental results for the total (left) and incident (right) IG-band wave heights for T01, T02, T03, T04, and T05. The colors indicate the numerical model considered, with XBeach-SB in red, XBeach-NH in blue and SWASH in green.

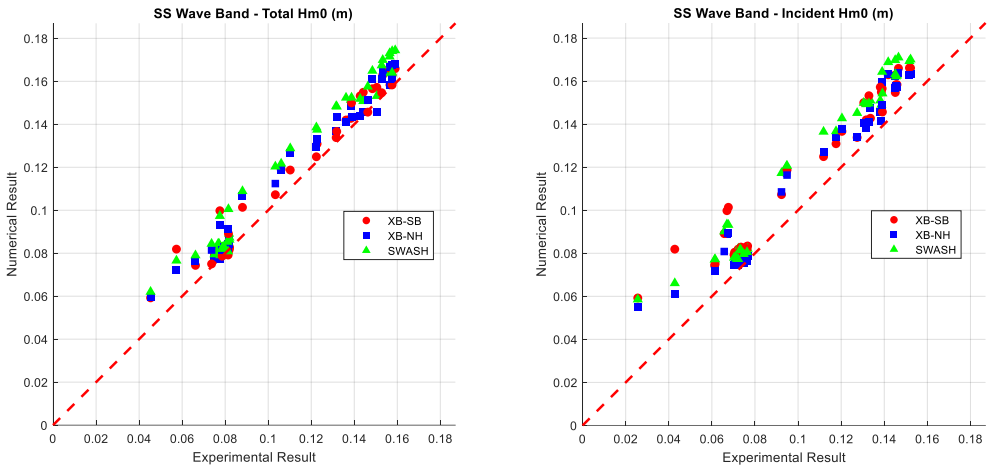

Figure 7 - Comparison of the total (left) and incident (right) SS-band wave heights for T01, T02, T03, T04, and T05. The colors indicate the numerical model considered, with XBeach-SB in red, XBeach-NH in blue, and SWASH in green.

For the total and incident IG waves, the numerical tools predict the significant IG wave height for values smaller than 2 cm. For larger IG wave heights, which occur when energetic SS waves are generated offshore, the correspondence is somewhat less. If a comparison is to be made, none of the three numerical models performs significantly better than the others in the IG waveband, except for T02 and T05, where SWASH overestimates observed IG waves as mentioned above. For the total and incident SS waves, the numerical tools perform better for relatively higher significant wave heights, which are found offshore and at the start of the slope in the seaward direction, i.e. seaward of the surf zone. XB-SB and XB-NH worked better than SWASH for this wave band for these cases.

In the figures given below (Figure 8 and Figure 9), percent error change with respect to local water depth for both total and incident significant wave height for both IG and SS wave bands is presented, respectively, for all wave sets (T01, T02, T03, T04, and T05). Percent error was calculated with the following equation for each of the nine measurement points:

$$\% \, Error = \frac{|H_{exp} - H_{num}|}{H_{exp}} * 100$$

where H_{exp} and H_{num} are the experimental and numerical significant wave heights.

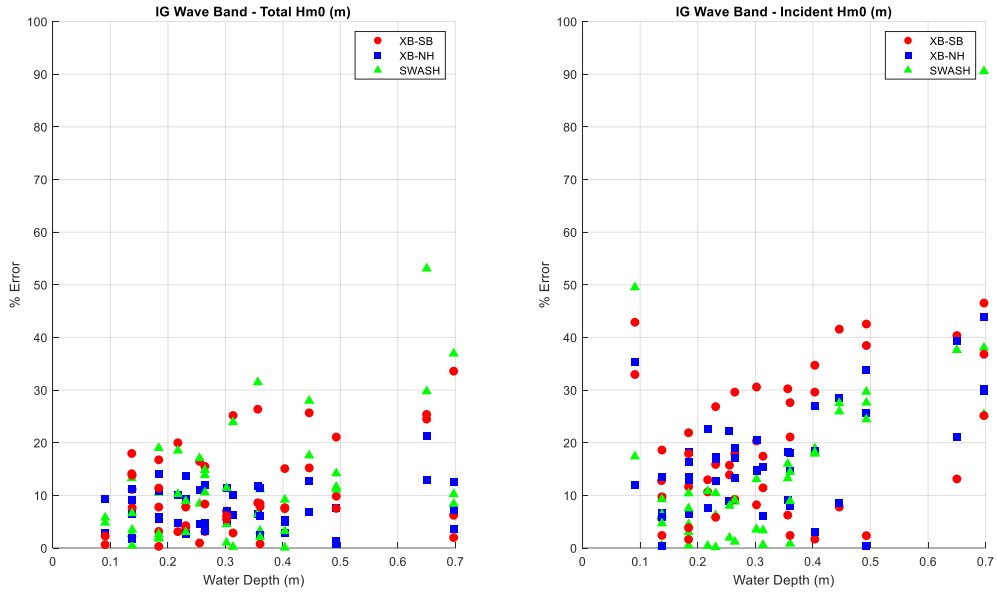

Figure 8 - Comparison of the relative errors for the total (left) and incident (right) IG-band wave heights for TO1, TO2, TO3, TO4, and TO5

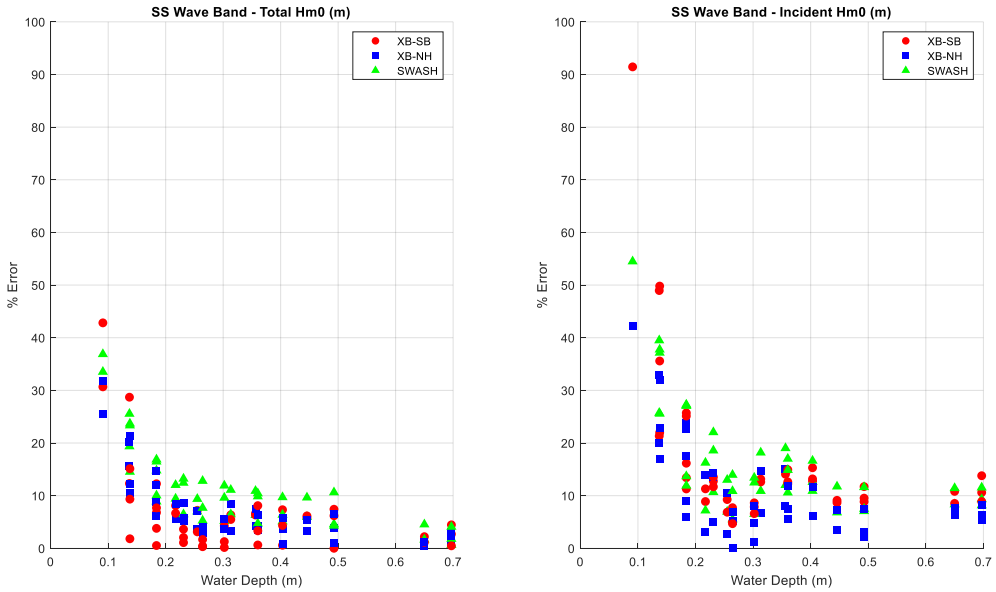

Figure 9 - Comparison of the relative errors for the total (left) and incident (right) SS-band wave heights for TO1, TO2, TO3, TO4, and TO5

For IG waves, there is no consistent trend between the water depth and the percent errors, but still, the errors are found to be generally smaller in the nearshore region compared to the offshore region for the total significant wave heights. For the water depth values smaller than 30 cm, the percent error values are not more than 20 %, but up to about 50% for deeper

water. If the numerical tools are compared, they performed both better and worse relative to each other at different water depths and in different cases.

For the SS wave band, there is a strong correlation between the water depth and the percent error values. For the total significant wave height, the percent errors are not higher than 20 % for water depths higher than 15 cm, and with decreasing water depth, error values go up to 40 %. For the incident significant wave height, the error values are worse but still relatively good for water depths higher than 20 cm, but increase to up to 90 % at the shallowest location. The error is caused by the fact that the calculated SS wave heights in the inner surf zone are systematically higher than the measured ones. Apparently, the wave energy is damped too little. Possible causes for the lower performance of the numerical models at the shallowest locations are discussed in Section 5.

If the numerical tools are compared by looking at the figures and the relative error tables, which are provided in Appendix A, XB-NH results seem to resemble the measurements more than the other models in every test case and almost at every water depth. Here, it should also be noted that T01 and T02 are the cases with 5 cm water depth at the toe of the structure. For T03, T04, and T05, this value is 10 cm. It can be clearly stated that with the increasing toe water depth, percent error values decrease, and the numerical tools present better matches with the experimental data.

In Table 1, mean wave overtopping ($m^3/s/m$) results observed for the Base Case configuration in the experiments and numerical simulations are given. For the experimental value, the average of the WG and MIC results is taken since these values are close.

Table 1 – Mean wave overtopping comparisons for all 5 wave sets considered for Base Case configuration

	Wave Overtopping ($m^3/s/m$)				
Method	BC_652_IR_8_16	BC_652_IR_16_28	BC_702_IR_8_16	BC_702_IR_16_16	BC_702_IR_16_28
Experiments	$5.98\ x\ 10^{-7}$	$1.87\ x\ 10^{-5}$	$3.17\ x\ 10^{-4}$	$4.44\ x\ 10^{-4}$	$3.95\ x\ 10^{-4}$
XB-SB	0	$4.32\ x\ 10^{-5}$	$1.36\ x\ 10^{-6}$	$1.00\ x\ 10^{-4}$	$5.57\ x\ 10^{-4}$
XB-NH	0	$5.57\ x\ 10^{-6}$	$1.16\ x\ 10^{-4}$	$2.09\ x\ 10^{-4}$	$6.25\ x\ 10^{-4}$
SWASH	0	$1.35\ x\ 10^{-5}$	$4.28\ x\ 10^{-4}$	$5.44\ x\ 10^{-4}$	$1.00\ x\ 10^{-3}$

Overall, the results for the mean wave overtopping from the SWASH simulations deviate by a factor of 1 to 3 from the experimental results. Deviations for XB-SB and XB-NH change with a factor from 0.01 to 3 and from 0.5 to 2, respectively. In general, SWASH presents closer results for mean wave overtopping except T05 (BC_702_IR_16_28); for this single case, XB-NH gives the closest result. For the T01 (BC_652_IR_8_16), no overtopping is observed in all three numerical models. In experiments, almost no overtopping (one or two individual wave overtopping) is observed either. The relatively small values for the mean wave overtopping from WG and MIC show no overtopping.

4.2 Raversijde configuration

In this part, the results for the Raversijde (R) configuration are presented. In the scope of the study, 3 different irregular wave cases were examined for this configuration by considering only one h_{toe}, which is 5 cm (2.25 m in model scale), in prototype scale. The names used for each case are given below.

- R_708_IR_8_16 ($\boldsymbol{T06}$)
- R_708_IR_16_16 ($\boldsymbol{T07}$)
- R_708_IR_16_28 ($\boldsymbol{T08}$)

Figures for mean water depth, total, and incident significant wave height evolution along the domain can be found in Appendix B.

To examine the total and significant wave heights for both IG and SS wave bands, the following graphs are given below (Figure 10 and Figure 11) for the wave height at nine different measurement locations of wave sets T06, T07, and T08.

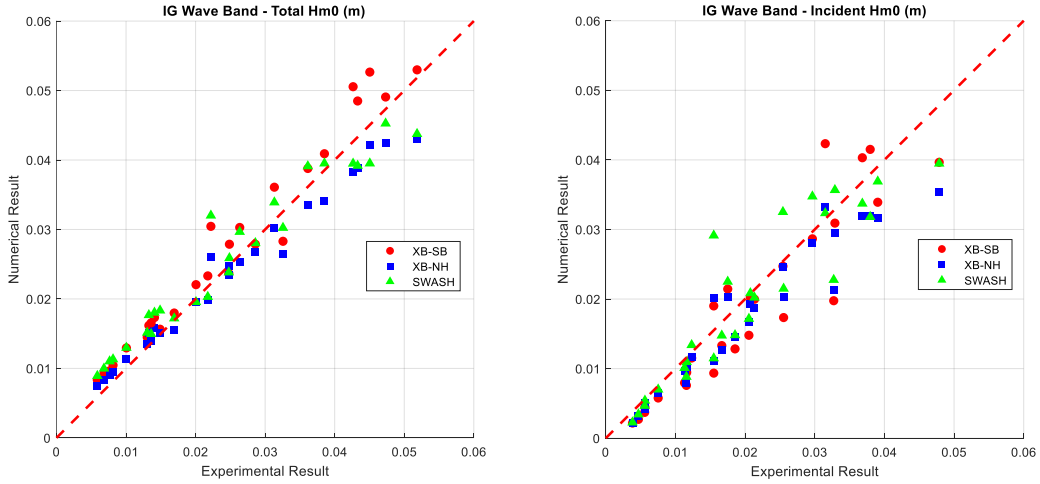

Figure 10 - Comparison of the total (left) and incident (right) IG-band wave heights for T06, T07, and T08

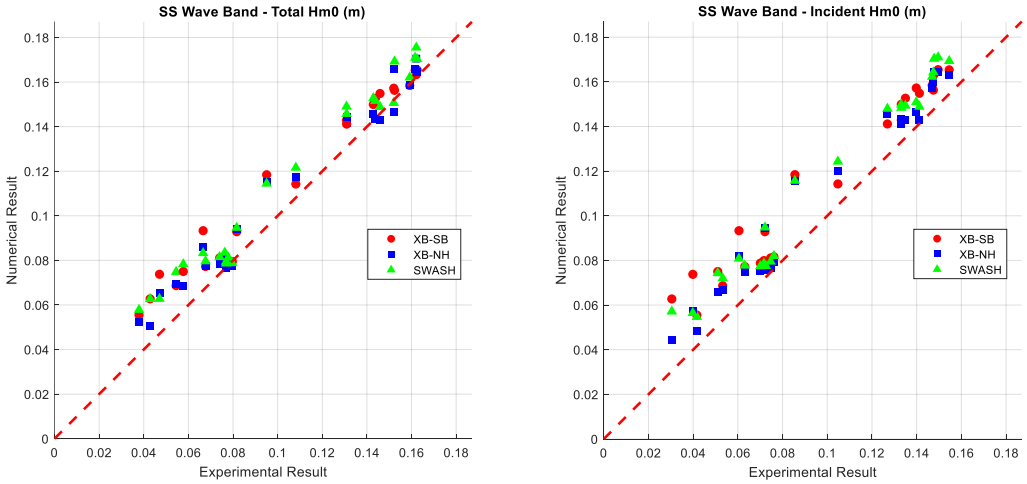

Figure 11 - Comparison of the total (left) and incident (right) SS-band wave heights for T06, T07, and T08

For the total and incident IG waves, the numerical tool results match experimental data best for significant IG wave height values smaller than 2 cm. In general, SWASH and XB-NH performed better than XB-SB in the IG wave band (see tables in Appendix B). For total and incident SS waves, the numerical tools performed better for relatively higher significant wave heights (offshore and the start of the slope in the seaward direction), and XB-NH worked better than the other numerical tools for this wave band for these cases.

In the figures given below (Figure 12 and Figure 13), the percent error change with respect to water depth for both total and incident significant wave height for both IG and SS wave bands is presented, respectively, for T06, T07, and T08 cases.

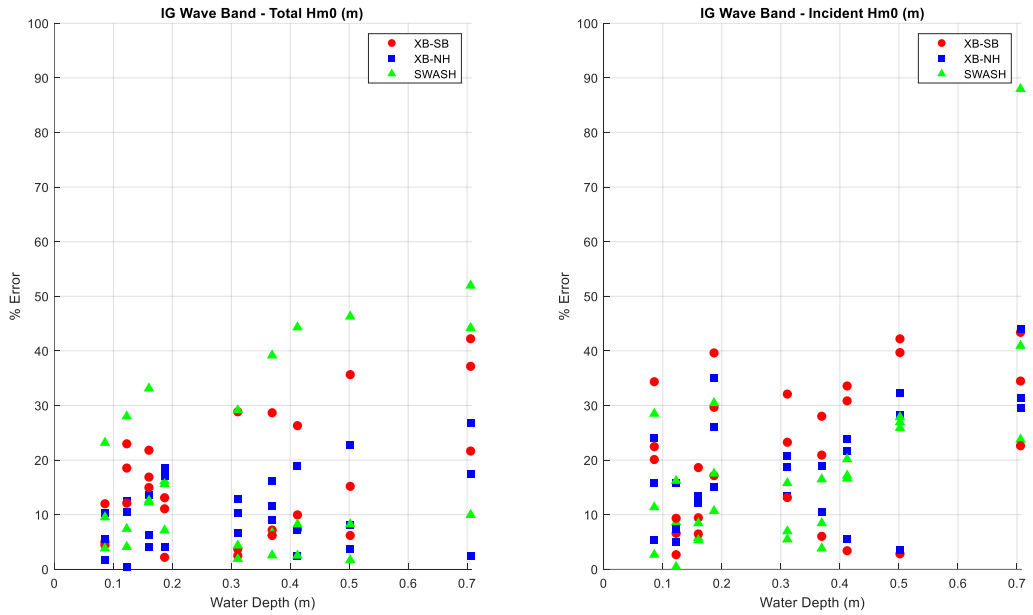

Figure 12 - Comparison of the relative errors for the total (left) and incident (right) IG-band wave heights for T06, T07, and T08

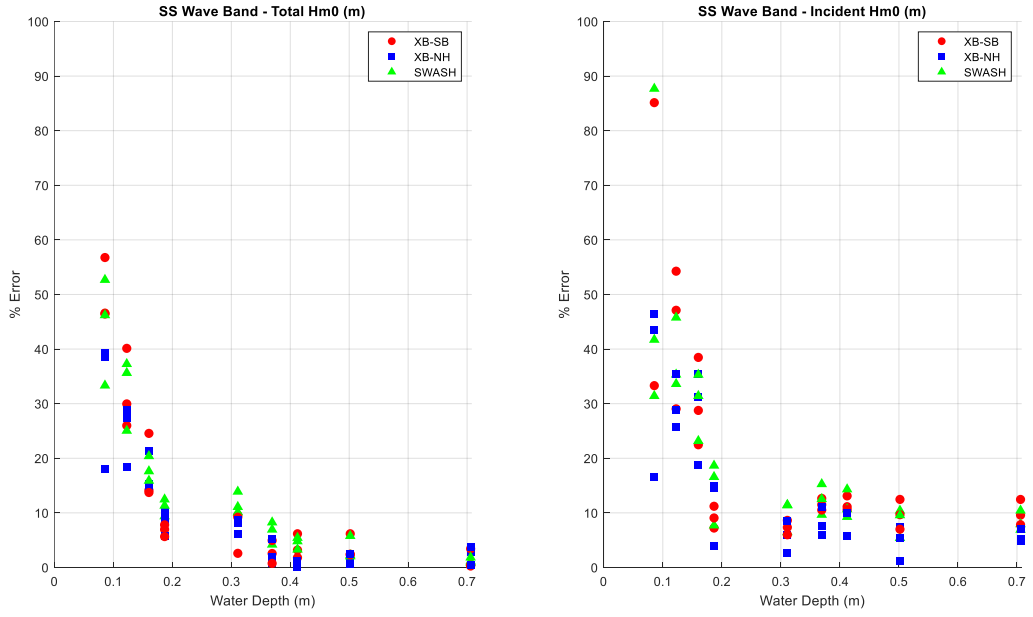

Figure 13 - Comparison of the relative errors for the total (left) and incident (right) SS-band wave heights for T06, T07, and T08

For IG waves, , the errors are, as for the Base Case, generally smaller in the nearshore region compared to the offshore region for both the total and incident significant wave heights. For the water depth values smaller than 50 cm, the percent error values are not more than 45 %

for the total significant wave height values. For the incident IG significant wave height, errors are slightly higher in general, except in the offshore area. Overall, the different numerical models performed similarly in these cases.

For the SS wave band, the percent error values for both the total and incident wave heights increase when the depth decreases. For the total significant wave height, the percent errors are not higher than 20 % for the water depths higher than 15 cm, and with decreasing water depth, error values go up to 60 %. For incident significant wave heights, the values are worse but still relatively good for the water depths higher than 30 cm. If the numerical tools are compared, for the total and incident significant wave height, XB-NH results corresponded somewhat better to the measurements compared to the other models in general.

In Table 2, mean wave overtopping results observed for the Raversijde configuration in the experiments and numerical simulations are given. For the experimental value, the average of the WG and MIC results is taken since these values are close.

Table 2 - Mean wave overtopping comparisons for all 3 wave sets considered for the Raversijde configuration

	Wave Overtopping ($m^3/s/m$)		
Method	R_708_IR_8_16	R_708_IR_16_16	R_708_IR_16_28
Experiments	$1.70\ x\ 10^{-7}$	$1.79\ x\ 10^{-5}$	$9.49x10^{-5}$
XB-SB	$2.84\ x\ 10^{-6}$	$4.41\ x\ 10^{-5}$	$2.82x10^{-4}$
XB-NH	$5.51\ x\ 10^{-7}$	$6.59\ x\ 10^{-6}$	$1.73x10^{-5}$
SWASH	$7.38\ x\ 10^{-6}$	$7.05\ x\ 10^{-5}$	$1.88x10^{-5}$

Overall, the results for the mean wave overtopping from the XB-NH simulations deviate by a factor of 0.2 to 5.5 from the experimental results. Deviations for XB-SB and SWASH change with a factor from 2.5 to 17 and from 0.2 to 43, respectively. In general, XB-NH presents closer results for mean wave overtopping except for T08 (R_708_IR_16_28); for this single case, SWASH gives the closest result.

4.3 Katwijk configuration

In this part, the results for the Katwijk (K) configuration are presented. In the scope of the study, 3 different irregular wave cases were examined for this configuration by considering only one h_{toe}, which is 5 cm in the tests (2.25 m at full scale). The names used for each case are given below.

- K_708_IR_8_16 ($\boldsymbol{T09}$)
- K_708_IR_16_16 ($\boldsymbol{T10}$)
- K_708_IR_16_28 ($\boldsymbol{T11}$)

Figures for mean water depth, total, and incident significant wave height evolution along the domain can be found in Appendix C.

To examine the total and significant wave heights for both IG and SS wave bands, the following graphs are given below (Figure 14 and Figure 15) for the wave height at nine different measurement locations of wave sets T09, T10, and T11.

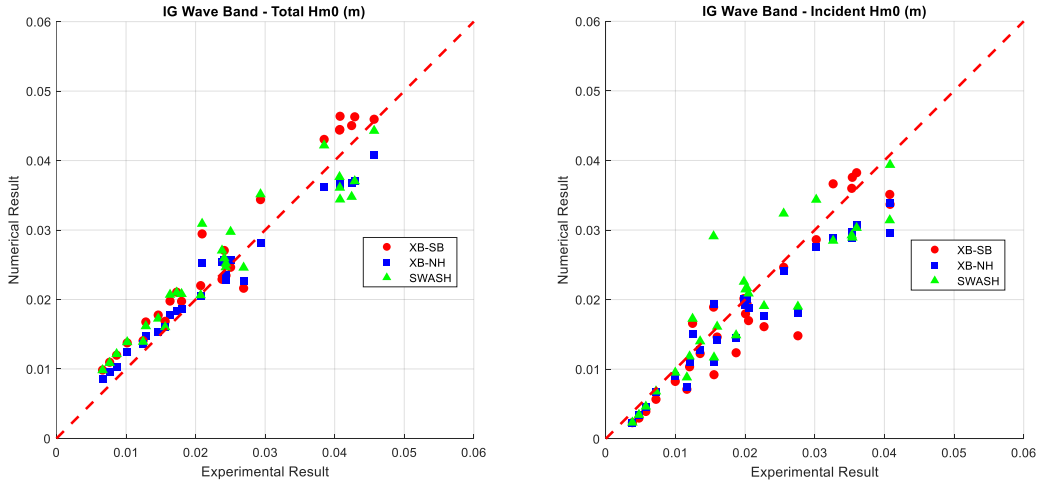

Figure 14 - Comparison of the total (left) and incident (right) IG-band wave heights for T09, T10, and T11

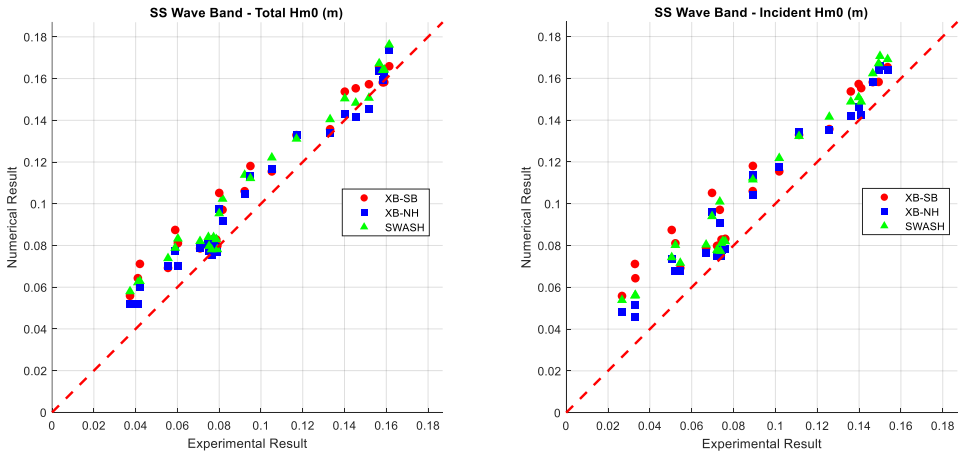

Figure 15 - Comparison of the total (left) and incident (right) SS-band wave heights for T06, T07, and T08

Overall, the observed behavior for the Katwijk cases is very similar to the Base Case and Raversijde in terms of distribution of the errors over the domain for the IG and SS wave heights, with more accurate numerical model predictions for the least energetic wave cases (smaller wave heights). The 3 numerical models are similarly accurate in this case again. A more detailed comparisons of the error metrics (see tables in Appendix C) reveal that SWASH and XB-NH performed slightly better than XB-SB in the IG wave band and that XB-NH worked slightly better than the other numerical tools for the SS waves.

In the figures given below (Figure 16 and Figure 17), percent error change with respect to water depth for both total and incident significant wave height for both IG and SS wave bands is presented, respectively, for T09, T10, and T11 cases.

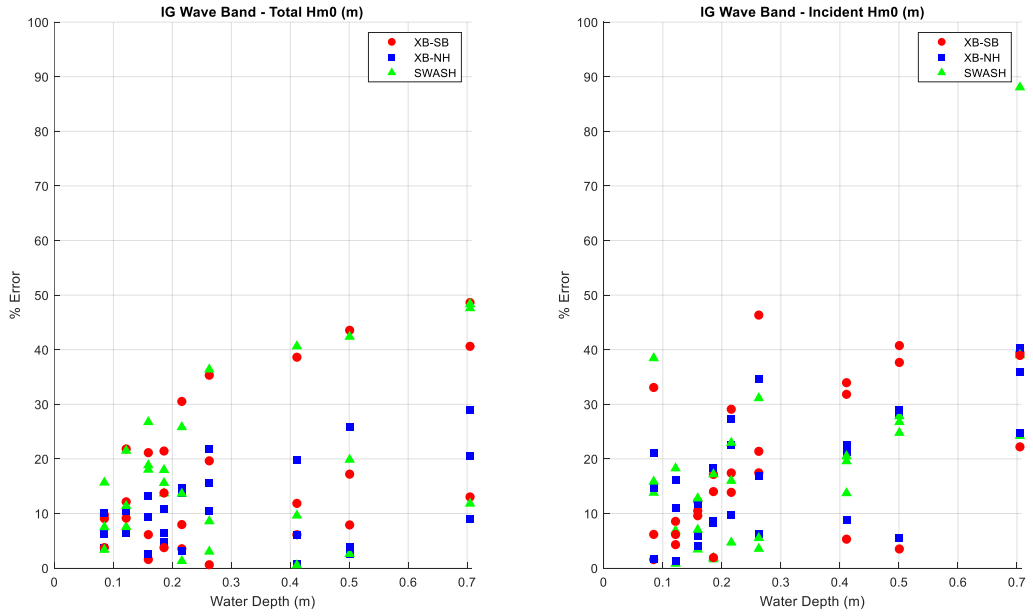

Figure 16 - Comparison of the relative errors for the total (left) and incident (right) IG-band wave heights for T09, T10, and T11

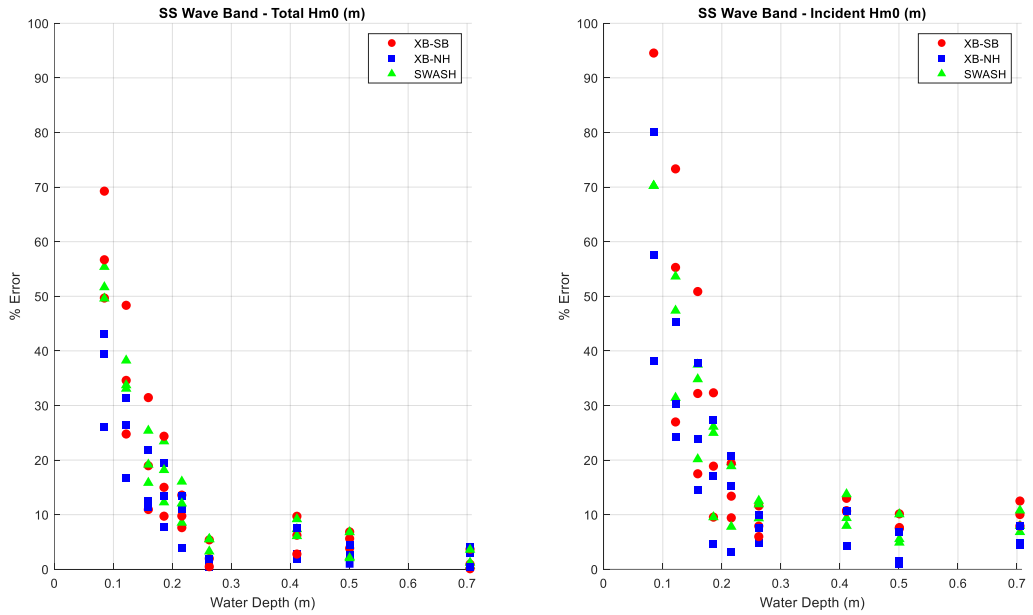

Figure 17 - Comparison of the relative errors for the total (left) and incident (right) SS-band wave heights for T09, T10, and T11

For the water depth values smaller than 50 cm, for the total IG wave height, the percent error values reach up to 40 %. For the incident IG significant wave height, errors are slightly higher in general, except in the offshore area.

For the SS wave band, there is again a strong correlation between the water depth and the percent error values. For the total significant wave height, the percent errors are less than 20 % for the water depths higher than 15 cm, and with decreasing water depth, error values go up to 70 %. For the total SS wave height, percent errors reach values close to 100 %, which is too much for a validation study.

In the table below (Table 3), mean wave overtopping results observed for the Katwijk configuration in the experiments and numerical simulations are given. For the experimental value, the average of the WG and MIC results is taken since these values are close.

Table 3 - Mean wave overtopping comparisons for all 3 wave sets considered for the Katwijk configuration

	Wave Overtopping ($m^3/s/m$)		
Method	**K_708_IR_8_16**	**K_708_IR_16_16**	**K_708_IR_16_28**
Experiments	$1.25\ x\ 10^{-6}$	$1.08\ x\ 10^{-5}$	$6.04\ x\ 10^{-5}$
XB-SB	$4.85\ x\ 10^{-6}$	$5.32\ x\ 10^{-5}$	$2.41\ x\ 10^{-4}$
XB-NH	$1.67\ x\ 10^{-6}$	$8.31\ x\ 10^{-6}$	$9.26\ x\ 10^{-5}$
SWASH	$1.24\ x\ 10^{-5}$	$6.95\ x\ 10^{-5}$	$1.98\ x\ 10^{-4}$

Overall, the results for the mean wave overtopping from the XB-NH simulations deviate by a factor of 0.75 to 4 from the experimental results. Deviations for XB-SB and SWASH change with a factor from 4 to 5 and from 3 to 10, respectively. In general, XB-NH presents closer results for mean wave overtopping for all considered cases for the Katwijk configuration.

5. Discussion

In this section of the report, the results are discussed, and possible reasons for observing higher errors for significant wave height and mean wave overtopping parameters are presented.

Mean overtopping discharge is known for having a large scatter, and the stochastic uncertainty is significantly higher for very shallow foreshores ($0.3 < h/H_{m0,deep} < 1$, Hofland et al., 2017) compared to shallow and deep water conditions. According to EurOtop (2018, Section 5.3.2), in shallow foreshore conditions ($1 < h/H_{m0,deep} < 4$), a difference within a factor of 2 to 3 falls within the standard scatter limits. Furthermore, differences ranging from a factor of 2.5 for low freeboards to as much as 20 for large freeboards (low overtopping rates) are typical in empirical predictions. Moreover, the exact scatter for very shallow foreshores is not known. So, the observed differences in mean wave overtopping results do not necessarily indicate a fundamental discrepancy between the numerical model and experimental results.

In addition to this, these observed differences may have been caused by two more reasons. The first one is that higher significant wave heights are observed in both IG and SS wave bands in the nearshore region of the domain in the numerical models compared to the experimental results. Mean wave overtopping ($m^3/s/m$) depends on the significant wave height at the toe of the structure, and this situation is one of the ways to explain the observed higher mean overtopping rates in the numerical tools. The second reason can be stated as the minimum water layer thickness parameter in the numerical tools. In these models, overtopping (or discharge in m^2/s) is computed as the multiplication of the flow velocity (m/s) and water layer thickness (m) at any point. The water layer thickness parameter defines the minimum water depth value in the model, even if there is no overtopping at that moment. This minimum value is 5 mm for XB-SB and XB-NH and 0.05 cm for SWASH, which could be significant when compared to the actual thickness of the overtopping layer in the lab. These default values can be reduced in the following studies.

In terms of the significant wave heights, scale effects, and breaking parameters could explain (part of) the mismatches in the results. Using another wave breaking methodology or parameters in the breaking models may lead to a better agreement between experimental and numerical results.

The scale effect consists of three components, which are viscous stress due to the fluid, bed friction, and sidewall friction. The effect of the viscous forces is higher than their effect in real life. This effect may have played a role in observing smaller, significant wave heights in the nearshore region in the experimental output.

Bed friction and sidewall friction are also crucial in terms of the scale effect. In the cross-shore (1D) numerical models, the sidewall friction could not be mimicked. In the simulations, the bed friction coefficient was taken as 0.01, which is an acceptable value for a smooth plywood bed. Also, for bed friction, the Manning equation was applied. Changing this formulation with another one, such as the White-Colebrook method, including the viscous effects on bed shear stress, may help to obtain more similar results between the experimental and numerical results. Alternatively, simply increasing the bed friction coefficient (n) may help, either. To see the effect of the bed friction coefficient on the results, additional simulations were carried out for one of the considered cases, which is BC_702_IR_16_16 (**T04**). In these simulations, the Manning formulation was applied as it was considered in other cases, but in these simulations, bed friction was increased to 0.03. The results of these simulations and their comparison with the main T04 (with n = 0.01 with the Manning formulation) are presented in the following figures (Figure 18 and Figure 19). In these figures, comparisons of the evolution of significant wave heights in the SS wave band for total and incident time series are given, respectively.

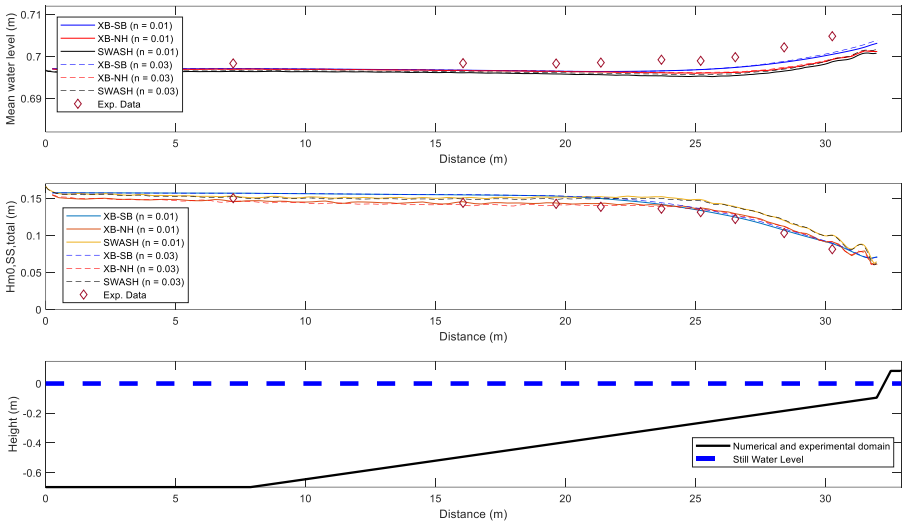

Figure 18 – Comparison for BC_702_IR_16_16 on total wave heights in the SS wave-band ($H_{m0,ss,incident}$) for two different bed friction values

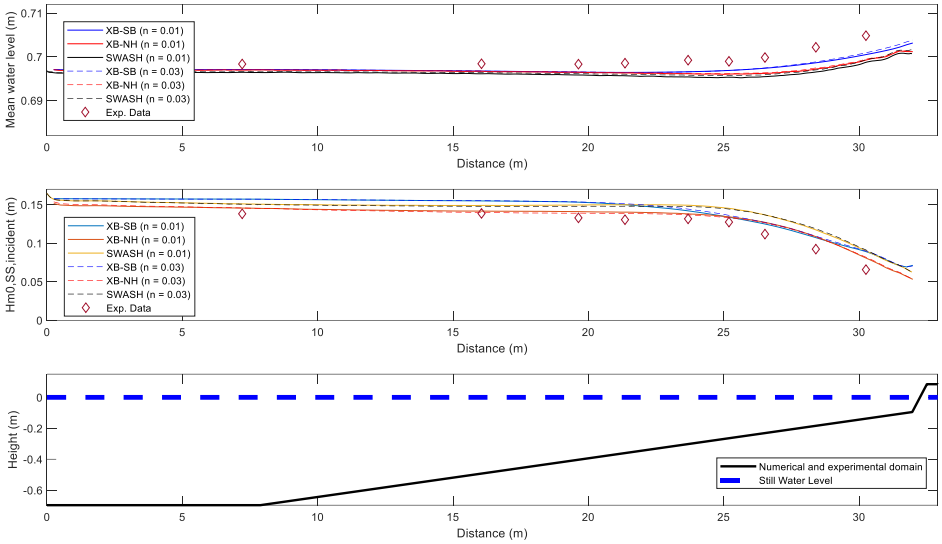

Figure 19 - Comparison for BC_702_IR_16_16 on incident wave heights in the SS wave-band ($H_{m0,ss,incident}$) for two different bed friction values

No significant difference were observed in terms of total and incident wave heights for the two different bed friction values considered. It was expected that increased bed friction (n = 0.03) would lead to decreasing nearshore significant wave heights, as it is an energy sink. However, nearshore significant wave heights on the SS wave band were seen to increase somewhat with the increasing friction factor. In light of this finding, changing the bed friction formulation may be more helpful for the following studies than simply altering the coefficients.

6. Conclusion

This study was carried out in the scope of WP12 – D12.4. Within the scope of this task, TU Delft has conducted, in close collaboration with UGent-E, a numerical modelling study to evaluate the performance of the numerical tools XBeach-SB, XBeach-NH, and SWASH using the hydrodynamic data set from the first experimental campaign described in DuneFront deliverable D12.1. The ultimate objective of this task is to calibrate and validate the aforementioned numerical models using the collected experimental data set, determine which of these models (or a combination thereof) is the most accurate for modeling wave–DD–Hybrid NbS interactions, and develop a numerical modeling methodology incorporating best practices. In this specific deliverable, the ability of the three aforementioned numerical models to reproduce sea-swell and infragravity wave transformation, mean water depths, and mean overtopping discharge over an eroded DD-Hybrid NbS is assessed. Simulations were conducted for a selection of eleven irregular wave sets from the experiments for the three tested configurations. In this initial validation study, several parameters, which are the mean water depth, incident and total significant wave height of both IG and SS waves, and mean wave overtopping, were considered, and results from the simulation outputs and the experimental data were compared for these parameters.

For mean water depth, all three numerical tools presented reasonable and similar results. Larger discrepancies are observed for the SS and IG significant wave heights. When looking at the SS significant wave heights, the relative error values tend to increase as the water depth decreases, and that for all 3 numerical models. Even though a good match and acceptable results are seen for significant wave heights for the SS wave band in the offshore part of the domain and at the following 6 WGs through the slope, there are significant relative errors for the last two wave gauges at the nearshore. An important source of mismatch for the SS wave band is the overall underestimation of the SS wave height decay in the surf zone of the numerical domain.

These relatively higher errors may be caused by the scale effects of the physical model, such as bed friction, sidewall friction, and viscous stresses, or the choice of breaking formulations in the numerical model. As it is mentioned in the previous section, a different bed friction coefficient (n) was also considered for one of the cases to see if this could improve the results, but it did not lead to any significant change. It is recommended that other bed friction and wave breaking formulations be considered in future studies.

For the total and incident IG waves, better (relative) matches between numerical models and data are seen for the nearshore region compared to the offshore region, where the smaller IG wave heights lead to higher relative error values.

For the mean wave overtopping comparisons, there are differences between the experimental and numerical results, but these differences do not necessarily indicate a fundamental

discrepancy between the numerical model and experimental results since the accepted large scatter limits in EurOtop (2018) are largely due to the stochastic nature of wave overtopping. In addition to this, these observed differences may have been caused by two more reasons. One of the reasons for this situation is observing higher significant wave heights at the dike toe in the numerical models. Another reason is that, as it is mentioned in the Discussion part, default values for water layer thickness are higher than zero even for non-overtopping moments on the dike crest, in the numerical simulation results. Not only the water layer thickness, but flow velocity is crucial at this point for numerical simulation results, and this topic needs to be further studied.

Despite the higher error values, it should also be noted that, for total and incident significant wave heights in both IG and SS wave bands, the XB-NH numerical tool gives slightly better validation results compared to XB-SB and SWASH for the specific cases considered. For mean wave overtopping, XB-NH and SWASH work better than XB-SB for the cases considered in the scope of this study.

Finally, it should be noted that, in the scope of this deliverable, experimental data gathered during the first experimental campaign of WP12 were used to validate and calibrate the XBeach and SWASH numerical tools, which means that the validation was limited to hydrodynamic aspects. For a better understanding of the ability of these models to describe the functioning of DD-Hybrid NbS during extreme conditions, the experiment results from the following experimental campaigns (D12.2 and D12.3, taking place in the coming year) should also be considered to choose the best numerical tool (or a combination thereof) for the modeling of the hydro-structure-morphodynamic response of DD–Hybrid NbS during extreme conditions.

References

Buckley, M. L., Lowe, R. J., Hansen, J. E., & Van Dongeren, A. R. (2015). Dynamics of wave setup over a steeply sloping fringing reef. *Journal of Physical Oceanography*, *45*(12), 3005-3023.

Daly, C., Roelvink, D., van Dongeren, A., de Vries, J. V. T., & McCall, R. (2012). Validation of an advective-deterministic approach to short wave breaking in a surf-beat model. *Coastal Engineering*, *60*, 69-83.

Delft University of Technology. (n.d.). *SWASH user manual (Version 11.01A)*. Delft University of Technology.

Deltares, UNESCO-IHE, & TU Delft. (2024). *XBeach: Hydrodynamics and morphological impacts of storms on beaches, dunes, and barrier islands* (Release XBeach 1.24.6057 Halloween). Deltares.

EurOtop (2018). Manual on wave overtopping of sea defences and related structures. An overtopping manual largely based on European research, but for worldwide application. Second Edition.

Guza, R. T., Thornton, E. B., & Holman, R. A. (1984). Swash on steep and shallow beaches. *Coastal Engineering Proceedings*, (19), 48-48.

Hasselmann, K. (1962). On the non-linear energy transfer in a gravity wave spectrum. *Journal of Fluid Mechanics*, 12(4), 481–500.

Hofland, B., Chen, X., Altomare, C., & Oosterlo, P. (2017). Prediction formula for the spectral wave period Tm-1, 0 on mildly sloping shallow foreshores. *Coastal Engineering*, *123*, 21-28.

Holthuijsen, L. H., Booij, N., & Herbers, T. H. C. (1989). A prediction model for stationary, short-crested waves in shallow water with ambient currents. *Coastal engineering*, *13*(1), 23-54.

Longuet-Higgins, M. S., & Stewart, R. W. (1962). Radiation stress and mass transport in gravity waves, with application to 'surf beats'. *Journal of Fluid Mechanics*, *13*(4), 481-504.

Longuet-Higgins, M. S., & Stewart, R. W. (1964, August). Radiation stresses in water waves; a physical discussion, with applications. In *Deep sea research and oceanographic abstracts* (Vol. 11, No. 4, pp. 529-562). Elsevier.

Nairn, R. B., Roelvink, J. A., & Southgate, H. N. (1990). Transition zone width and implications for modelling surfzone hydrodynamics. In *Coastal engineering 1990* (pp. 68-81).

Phillips, O. M. (1966). *The dynamics of the upper ocean* (Vol. 2). Cambridge: Cambridge university press.

Roelvink, J. A. (1993). Dissipation in random wave groups incident on a beach. *Coastal Engineering*, *19*(1-2), 127-150.

Roelvink, D., Reniers, A., Van Dongeren, A. P., De Vries, J. V. T., McCall, R., & Lescinski, J. (2009). Modelling storm impacts on beaches, dunes and barrier islands. *Coastal engineering*, *56*(11-12), 1133-1152.

Sevindik, Adeli, Tissier, Gruwez, Hofland, Troch, Lojek (2025) Dutch Physical model of the Demonstrator(s), focus: wave-dike interactions. DuneFront Project Deliverable 12.1, Version 1.0.

Stive, M. J., & De Vriend, H. J. (1995). Shear stresses and mean flow in shoaling and breaking waves. In *Coastal Engineering 1994* (pp. 594-608).

Svendsen, I. A. (1984). Wave heights and set-up in a surf zone. *Coastal engineering*, *8*(4), 303-329.

Zijlema, M., Stelling, G., & Smit, P. (2011). SWASH: An operational public domain code for simulating wave fields and rapidly varied flows in coastal waters. *Coastal Engineering*, *58*(10), 992-1012.

Appendix – A

BC_652_IR_8_16

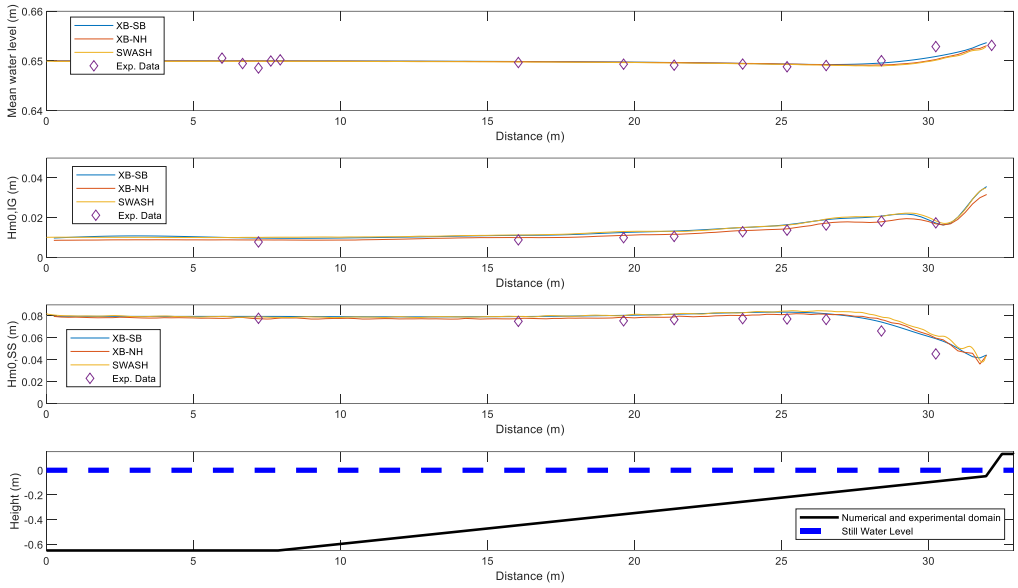

Figure 20 - Mean water depth (first panel) and total wave height for the infragravity (second panel) and sea-swell (third panel) waves along the domain for BC_652_IR_8_16 (T01) for the three numerical (colored lines) and for the data (diamonds).

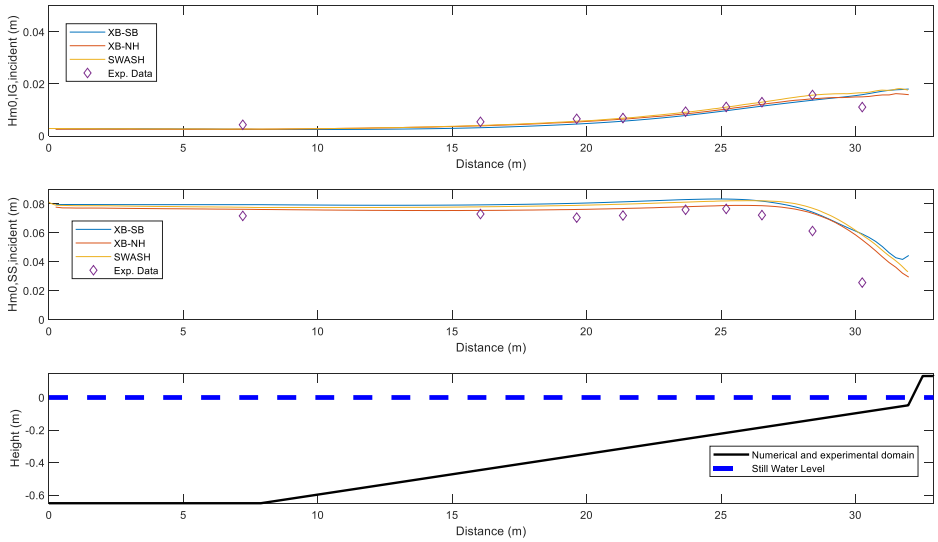

Figure 21 - Incident wave height for the infragravity (first panel) and sea-swell (second panel) waves along the domain for BC_652_IR_8_16 (T01) for the three numerical (colored lines) and for the data (diamonds).

Table 4 - Total wave heights ($H_{m0,IG,total}$) and percent errors for the IG wave band for BC_652_IR_8_16 (T01)

	WG	SB	NH	SWASH	% Error (SB)	% Error (NH)	% Error (SWASH)
WG-3	0.78	0.98	0.88	1.01	25.38	12.99	29.75
WG-6	0.88	1.11	1.00	1.13	25.67	12.78	27.96
WG-7	0.99	1.26	1.11	1.31	26.36	11.70	31.47
WG-8	1.06	1.33	1.17	1.31	25.17	10.09	23.90
WG-9	1.29	1.50	1.35	1.51	16.46	4.59	17.06
WG-10	1.37	1.65	1.44	1.63	19.98	4.78	18.49
WG-11	1.63	1.90	1.72	1.94	16.75	5.83	18.98
WG-12	1.82	2.08	1.79	2.07	14.11	1.68	13.26
WG-13	1.74	1.73	1.69	1.84	0.64	2.83	5.78

Table 5 - Total wave heights ($H_{m0,SS,total}$) and percent errors for the SS wave band for BC_652_IR_8_16 (T01)

	WG	SB	NH	SWASH	% Error (SB)	% Error (NH)	% Error (SWASH)
WG-3	7.78	7.95	7.74	7.91	2.21	0.48	1.65
WG-6	7.50	7.94	7.75	7.95	5.78	3.27	5.95
WG-7	7.55	8.05	7.86	8.02	6.62	4.15	6.33
WG-8	7.66	8.15	7.91	8.15	6.35	3.27	6.46
WG-9	7.74	8.30	8.03	8.29	7.21	3.65	7.00
WG-10	7.71	8.34	8.14	8.44	8.11	5.54	9.43
WG-11	7.67	8.20	8.15	8.44	6.80	6.16	10.04
WG-12	6.62	7.43	7.65	7.90	12.31	15.55	19.37
WG-13	4.53	5.92	5.97	6.20	30.67	31.75	36.88

Table 6 - Incident wave heights ($H_{m0,IG,incident}$) and percent errors for the IG wave band for BC_652_IR_8_16 (T01)

	WG	SB	NH	SWASH	% Error (SB)	% Error (NH)	% Error (SWASH)
WG-3	0.43	0.26	0.26	0.27	40.35	39.35	37.59
WG-6	0.55	0.32	0.39	0.40	41.57	28.40	25.93
WG-7	0.66	0.46	0.54	0.57	30.24	18.24	13.24
WG-8	0.69	0.57	0.65	0.69	17.43	6.01	0.58
WG-9	0.93	0.79	0.85	0.92	15.73	8.91	1.95
WG-10	1.12	0.97	1.03	1.11	12.95	7.65	0.42
WG-11	1.30	1.15	1.22	1.31	11.65	6.43	0.48
WG-12	1.58	1.38	1.43	1.57	12.78	9.42	0.50

WG-13	1.11	1.59	1.50	1.66	42.88	35.38	49.51

Table 7 - Incident wave heights ($H_{m0,SS,incident}$) and percent errors for the SS wave band for BC_652_IR_8_16 (TO1)

	WG	SB	NH	SWASH	% Error (SB)	% Error (NH)	% Error (SWASH)
WG-3	7.17	7.95	7.63	7.77	10.81	6.37	8.34
WG-6	7.30	7.94	7.55	7.80	8.68	3.43	6.82
WG-7	7.05	8.05	7.62	7.90	14.06	8.01	12.02
WG-8	7.20	8.15	7.68	7.98	13.16	6.70	10.89
WG-9	7.60	8.30	7.81	8.13	9.26	2.74	6.95
WG-10	7.66	8.34	7.89	8.21	8.89	3.04	7.18
WG-11	7.23	8.20	7.88	8.22	13.41	9.02	13.69
WG-12	6.13	7.43	7.35	7.70	21.33	19.97	25.72
WG-13	2.56	5.92	5.51	5.85	131.30	115.37	128.62

BC_652_IR_16_28

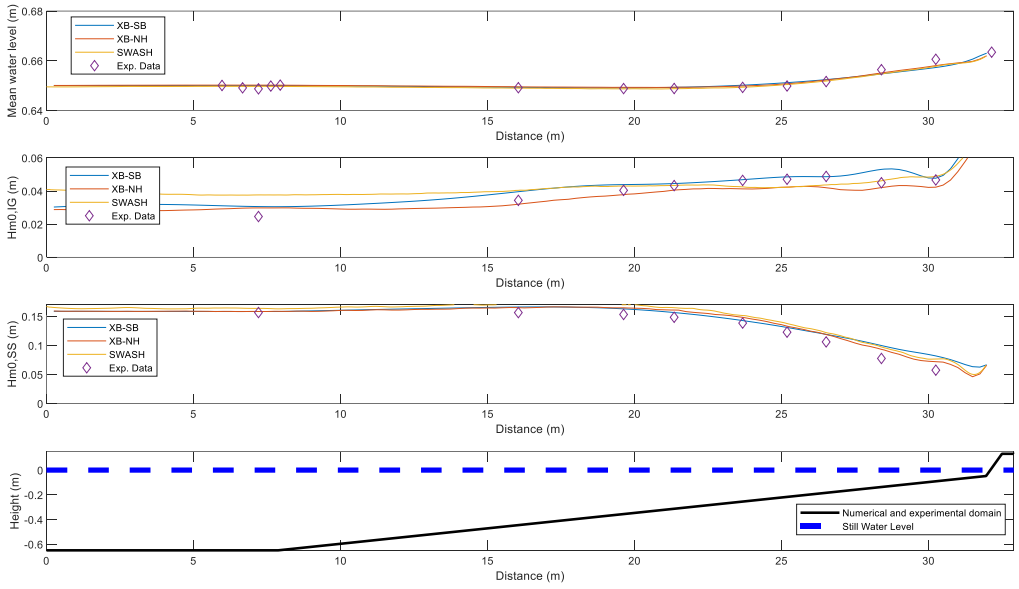

Figure 22 - Mean water depth (first panel) and total wave height for the infragravity (second panel) and sea-swell (third panel) waves along the domain for BC_652_IR_16_28 (TO2) for the three numerical (colored lines) and for the data (diamonds).

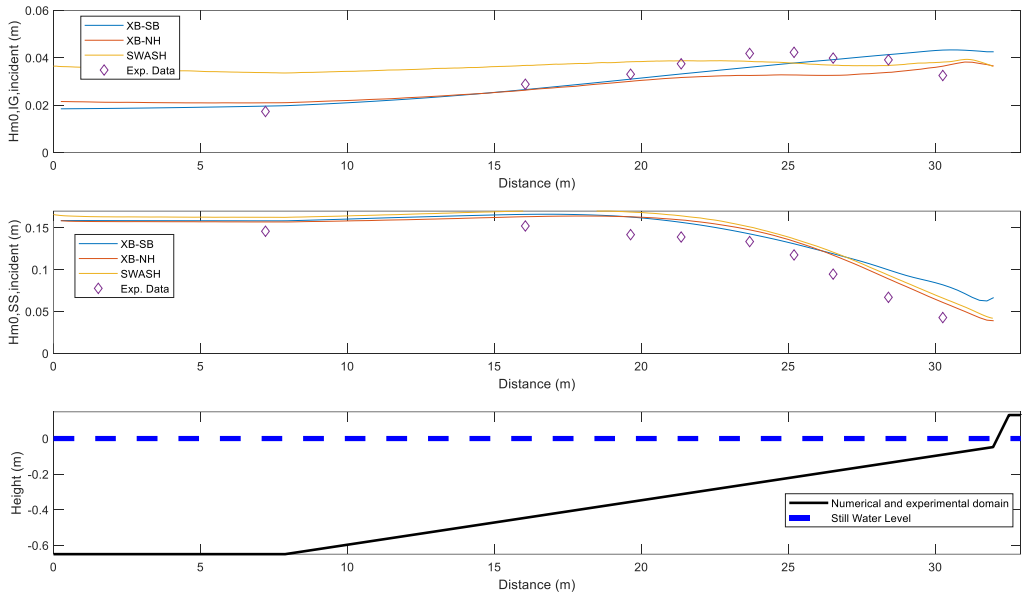

Figure 23 - Incident wave height for the infragravity (first panel) and sea-swell (second panel) waves along the domain for BC_652_IR_16_28 (T02) for the three numerical (colored lines) and for the data (diamonds).

Table 8 - Total wave heights ($H_{m0,IG,total}$) and percent errors for the IG wave band for BC_652_IR_16_28 (T02)

	WG	SB	NH	SWASH	% Error (SB)	% Error (NH)	% Error (SWASH)
WG-3	2.46	3.06	2.98	3.77	24.48	21.22	53.07
WG-6	3.44	3.96	3.20	4.04	15.21	6.78	17.58
WG-7	4.04	4.39	3.78	4.30	8.58	6.51	6.43
WG-8	4.33	4.45	4.06	4.34	2.86	6.25	0.21
WG-9	4.64	4.69	4.13	4.25	0.94	11.02	8.43
WG-10	4.71	4.86	4.24	4.23	3.11	10.06	10.23
WG-11	4.88	4.87	4.20	4.37	0.32	13.99	10.48
WG-12	4.50	5.31	4.21	4.62	17.95	6.48	2.65
WG-13	4.67	4.77	4.23	4.89	2.26	9.34	4.80

Table 9 - Total wave heights ($H_{m0,SS,total}$) and percent errors for the SS wave band for BC_652_IR_16_28 (TO2)

	WG	SB	NH	SWASH	% Error (SB)	% Error (NH)	% Error (SWASH)
WG-3	15.66	15.84	15.84	16.37	1.14	1.16	4.54
WG-6	15.64	16.61	16.50	17.15	6.16	5.45	9.64
WG-7	15.32	16.29	16.47	16.99	6.32	7.49	10.90
WG-8	14.84	15.66	16.09	16.49	5.47	8.40	11.10
WG-9	13.84	14.28	14.83	15.14	3.13	7.14	9.38
WG-10	12.27	13.09	13.31	13.75	6.66	8.47	12.03
WG-11	10.60	11.90	11.87	12.17	12.26	11.95	14.78
WG-12	7.75	9.98	9.32	9.73	28.70	20.21	25.54
WG-13	5.73	8.19	7.20	7.66	42.82	25.50	33.52

Table 10 - Incident wave heights ($H_{m0,IG,incident}$) and percent errors for the IG wave band for BC_652_IR_16_28 (TO2)

	WG	SB	NH	SWASH	% Error (SB)	% Error (NH)	% Error (SWASH)
WG-3	1.73	1.96	2.10	3.37	13.11	21.16	94.60
WG-6	2.88	2.66	2.63	3.68	7.78	8.63	27.51
WG-7	3.30	3.10	3.01	3.83	6.25	9.05	15.98
WG-8	3.75	3.32	3.17	3.87	11.43	15.41	3.35
WG-9	4.18	3.60	3.25	3.85	13.89	2.,18	8.00
WG-10	4.23	3.78	3.27	3.77	10.65	22.58	10.81
WG-11	3.99	3.92	3.26	3.69	1.65	18.24	7.52
WG-12	3.91	4.13	3.38	3.67	5.66	13.46	6.11
WG-13	3.25	4.32	3.64	3.82	32.95	12.06	17.39

Table 11 - Incident wave heights ($H_{m0,SS,incident}$) and percent errors for the SS wave band for BC_652_IR_16_28 (TO2)

	WG	SB	NH	SWASH	% Error (SB)	% Error (NH)	% Error (SWASH)
WG-3	14.59	15.84	15.71	16.26	8.53	7.63	11.43
WG-6	15.22	16.61	16.33	17.01	9.11	7.29	11.74
WG-7	14.18	16.29	16.32	16.88	14.87	15.08	19.02
WG-8	13.90	15.66	15.94	16.43	12.61	14.68	18.18
WG-9	13.36	14.28	14.76	15.10	6.86	10.48	13.01
WG-10	11.76	13.09	13.39	13.67	11.30	13.84	16.26
WG-11	9.47	11.90	11.73	12.05	25.73	23.89	27.28
WG-12	6.70	9.98	8.90	9.34	48.96	32.91	39.50
WG-13	4.28	8.19	6.09	6.61	91.44	42.28	54.49

BC_702_IR_8_16

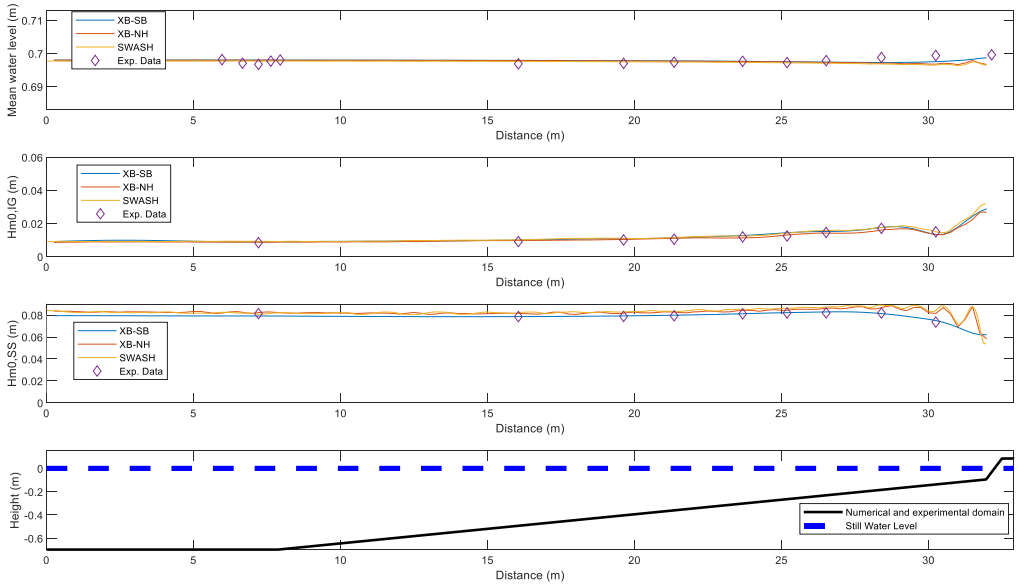

Figure 24 - Mean water depth (first panel) and total wave height for the infragravity (second panel) and sea-swell (third panel) waves along the domain for BC_702_IR_8_16 (T03) for the three numerical (colored lines) and for the data (diamonds).

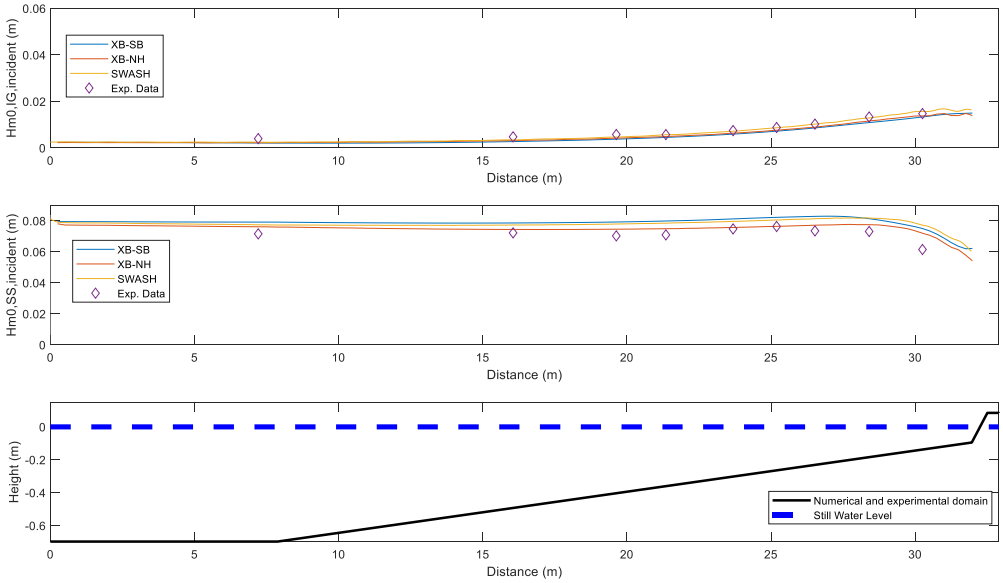

Figure 25 - Incident wave height for the infragravity (first panel) and sea-swell (second panel) waves along the domain for BC_702_IR_8_16 (T03) for the three numerical (colored lines) and for the data (diamonds).

Table 12 - Total wave heights ($H_{m0,IG,total}$) and percent errors for the IG wave band for BC_702_IR_8_16 (TO3)

	WG	SB	NH	SWASH	% Error (SB)	% Error (NH)	% Error (SWASH)
WG-3	0.84	0.89	0.87	0.93	6.21	3.57	10.22
WG-6	0.91	1.00	0.98	1.02	9.84	7.65	11.60
WG-7	1.01	1.09	1.04	1.10	7.67	2.90	9.17
WG-8	1.05	1.13	1.11	1.17	7.86	6.12	11.14
WG-9	1.19	1.28	1.13	1.25	6.99	5.11	4.53
WG-10	1.25	1.44	1.31	1.42	15.51	4.72	13.84
WG-11	1.46	1.52	1.42	1.58	4.24	2.64	8.31
WG-12	1.71	1.76	1.61	1.76	3.14	5.87	2.64
WG-13	1.50	1.33	1.33	1.51	11.12	11.13	0.46

Table 13 – Total wave heights ($H_{m0,SS,total}$) and percent errors for the SS wave band for BC_702_IR_8_16 (TO3)

	WG	SB	NH	SWASH	% Error (SB)	% Error (NH)	% Error (SWASH)
WG-3	8.14	7.92	8.23	8.09	2.71	1.14	0.63
WG-6	7.86	7.86	8.16	8.20	0.01	3.77	4.30
WG-7	7.88	7.92	8.17	8.28	0.58	3.74	5.11
WG-8	7.94	7.99	8.27	8.31	0.64	4.19	4.70
WG-9	8.11	8.12	8.44	8.53	0.15	4.01	5.18
WG-10	8.20	8.22	8.43	8.63	0.31	2.85	5.26
WG-11	8.20	8.29	8.63	8.73	1.08	5.23	6.46
WG-12	8.18	8.14	8.68	8.91	0.53	6.14	8.88
WG-13	7.37	7.50	8.15	8.44	1.81	10.58	14.53

Table 14 – Incident wave heights ($H_{m0,IG,incident}$) and percent errors for the IG wave band for BC_702_IR_8_16 (TO3)

	WG	SB	NH	SWASH	% Error (SB)	% Error (NH)	% Error (SWASH)
WG-3	0.40	0.21	0.23	0.25	46.52	43.95	38.04
WG-6	0.48	0.27	0.32	0.35	42.54	33.87	27.62
WG-7	0.58	0.38	0.42	0.47	34.71	27.03	18.93
WG-8	0.57	0.45	0.49	0.57	21.08	14.54	0.81
WG-9	0.75	0.59	0.64	0.72	20.34	14.72	3.51
WG-10	0.88	0.72	0.76	0.87	17.91	13.27	1.19
WG-11	1.02	0.86	0.89	1.03	15.87	12.69	0.15
WG-12	1.33	1.09	1.16	1.29	17.93	12.87	3.01
WG-13	1.48	1.33	1.38	1.57	9.73	6.74	6.41

Table 15 – Incident wave heights ($H_{m0,SS,incident}$) and percent errors for the SS wave band for BC_702_IR_8_16 (TO3)

	WG	SB	NH	SWASH	% Error (SB)	% Error (NH)	% Error (SWASH)
WG-3	7.16	7.92	7.62	7.74	10.60	6.38	8.16
WG-6	7.22	7.86	7.44	7.73	8.86	3.08	7.06
WG-7	7.03	7.92	7.46	7.79	12.74	6.12	10.91
WG-8	7.09	7.99	7.49	7.84	12.63	5.63	10.60
WG-9	7.48	8.12	7.57	7.96	8.64	1.24	6.52
WG-10	7.63	8.22	7.64	8.05	7.72	0.08	5.50
WG-11	7.35	8.29	7.72	8.13	12.75	4.99	10.67
WG-12	7.31	8.14	7.75	8.18	11.28	6.00	11.89
WG-13	6.15	7.50	7.20	7.72	21.98	17.06	25.56

BC_702_IR_16_16

Table 16 - Total wave heights ($H_{m0,IG,total}$) and percent errors for the IG wave band for BC_702_IR_16_16 (TO4)

	WG	SB	NH	SWASH	% Error (SB)	% Error (NH)	% Error (SWASH)
WG-3	1.69	1.73	1.57	1.84	1.98	7.30	8.39
WG-6	1.89	2.03	1.88	2.10	7.52	0.81	11.11
WG-7	2.27	2.44	2.16	2.27	7.47	4.98	0.06
WG-8	2.60	2.58	2.30	2.51	0.78	11.34	3.26
WG-9	2.85	2.69	2.64	2.88	5.47	7.10	1.01
WG-10	3.06	2.96	2.96	3.51	3.12	3.28	14.80
WG-11	3.18	3.05	2.88	3.27	3.93	9.32	3.01
WG-12	3.37	3.10	3.00	3.43	7.77	10.88	1.98
WG-13	2.43	2.24	2.38	2.59	7.67	1.93	6.61

Table 17 - Total wave heights ($H_{m0,SS,total}$) and percent errors for the SS wave band for BC_702_IR_16_16 (TO4)

	WG	SB	NH	SWASH	% Error (SB)	% Error (NH)	% Error (SWASH)
WG-3	15.05	15.72	14.59	15.32	4.46	3.02	1.79
WG-6	14.42	15.49	14.56	15.08	7.42	1.00	4.59
WG-7	14.28	15.32	14.39	15.18	7.33	0.79	6.37
WG-8	13.87	15.00	14.35	15.24	8.11	3.43	9.87
WG-9	13.62	14.20	14.12	15.24	4.28	3.69	11.91
WG-10	13.16	13.38	13.69	14.85	1.67	4.00	12.80
WG-11	12.24	12.49	12.94	13.86	2.06	5.75	13.22
WG-12	10.33	10.72	11.24	12.03	3.79	8.80	16.48
WG-13	8.15	8.91	9.15	10.05	9.34	12.22	23.34

Table 18 - Incident wave heights ($H_{m0,IG,incident}$) and percent errors for the IG wave band for BC_702_IR_16_16 (TO4)

	WG	SB	NH	SWASH	% Error (SB)	% Error (NH)	% Error (SWASH)
WG-3	1.21	0.77	0.85	0.90	36.80	30.18	25.41
WG-6	1.57	0.97	1.17	1.19	38.46	25.65	24.44
WG-7	1.87	1.32	1.52	1.54	29.60	18.49	17.91
WG-8	2.08	1.51	1.71	1.78	27.61	18.00	14.41
WG-9	2.53	1.76	2.02	2.20	30.58	20.42	13.07
WG-10	2.70	1.90	2.19	2.46	29.60	18.91	8.81
WG-11	2.73	1.99	2.26	2.56	26.85	17.23	6.20
WG-12	2.70	2.11	2.26	2.58	21.89	16.38	4.48
WG-13	2.31	2.26	2.31	2.53	2.39	0.39	9.26

Table 19 - Incident wave heights ($H_{m0,SS,incident}$) and percent errors for the SS wave band for BC_702_IR_16_16 (TO4)

	WG	SB	NH	SWASH	% Error (SB)	% Error (NH)	% Error (SWASH)
WG-3	13.81	15.72	14.56	15.10	13.79	5.39	9.32
WG-6	13.86	15.49	14.17	14.90	11.72	2.18	7.49
WG-7	13.29	15.32	14.10	14.96	15.30	6.12	12.59
WG-8	13.05	15.00	14.03	14.99	14.93	7.52	14.88
WG-9	13.16	14.20	13.80	14.93	7.88	4.87	13.41
WG-10	12.74	13.38	13.41	14.52	5.02	5.28	13.95
WG-11	11.18	12.49	12.71	13.65	11.69	13.62	22.05
WG-12	9.23	10.72	10.85	11.73	16.16	17.56	27.05
WG-13	6.57	8.91	8.08	9.02	35.58	22.94	37.15

BC_702_IR_16_28

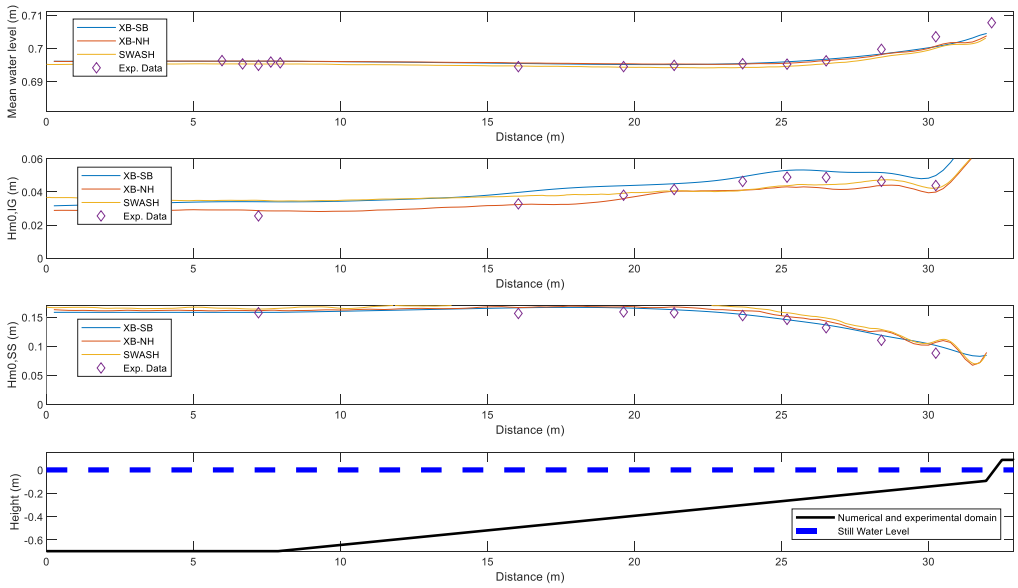

Figure 26 - Mean water depth (first panel) and total wave height for the infragravity (second panel) and sea-swell (third panel) waves along the domain for BC_702_IR_16_28 (T05) for the three numerical (colored lines) and for the data (diamonds).

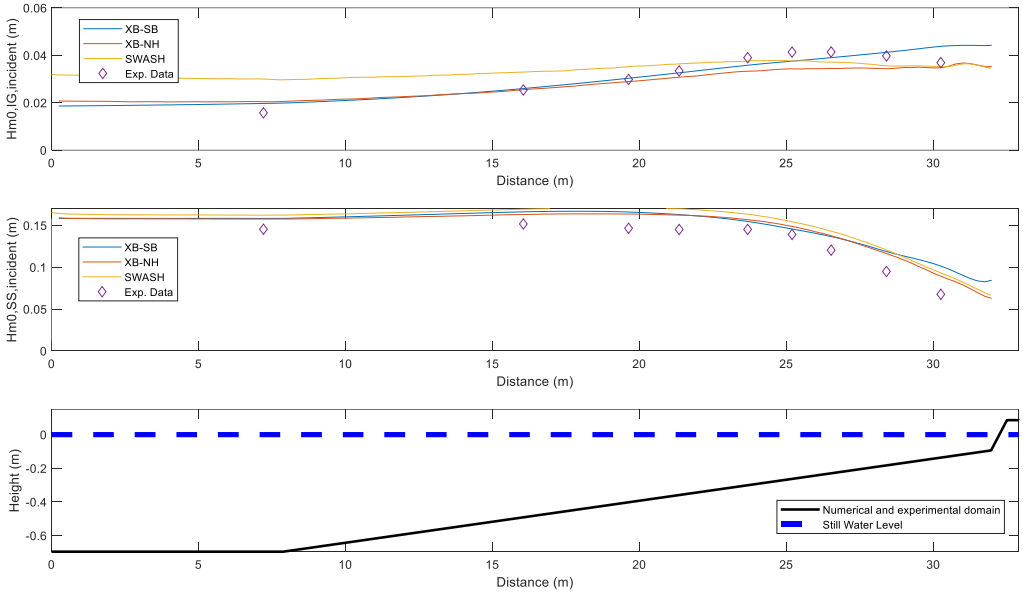

Figure 27 - Incident wave height for the infragravity (first panel) and sea-swell (second panel) waves along the domain for BC_702_IR_16_28 (T05) for the three numerical (colored lines) and for the data (diamonds).

Table 20 - Total wave heights ($H_{m0,IG,total}$) and percent errors for the IG wave band for BC_702_IR_16_28 (TO5)

	WG	SB	NH	SWASH	% Error (SB)	% Error (NH)	% Error (SWASH)
WG-3	2.55	3.40	2.87	3.49	33.59	12,49	36,93
WG-6	3.28	3.97	3.24	3.74	21.07	1.25	14,19
WG-7	3.80	4.37	3.60	3.92	15.08	5.24	3,21
WG-8	4.14	4.49	4.04	4.06	8.43	2.45	2,07
WG-9	4.63	4.91	4.10	4.10	6.14	11.37	11,41
WG-10	4.89	5.29	4.30	4.37	8.34	11.93	10,54
WG-11	4.87	5.25	4.21	4.44	7.77	13.62	8,91
WG-12	4.64	5.16	4.38	4.72	11.38	5.53	1,78
WG-13	4.38	4.99	3.99	4.23	13.81	9.03	3,46

Table 21 - Total wave heights ($H_{m0,SS,total}$) and percent errors for the SS wave band for BC_702_IR_16_28 (TO5)

	WG	SB	NH	SWASH	% Error (SB)	% Error (NH)	% Error (SWASH)
WG-3	15.76	15.83	16.12	16.40	0.47	2.31	4.08
WG-6	15.65	16.61	16.67	17.31	6.19	6.52	10.63
WG-7	15.90	16.59	16.81	17.45	4.35	5.71	9.70
WG-8	15.76	16.29	1676	17.41	3.32	6.36	10.43
WG-9	15.28	15.47	16.12	16.74	1.27	5.50	9.61
WG-10	14.63	14.57	15.12	15.75	0.43	3.36	7.68
WG-11	13.19	13.66	14.33	14.83	3.64	8.69	12.45
WG-12	11.02	11.87	12.65	12.88	7.69	14.70	16.86
WG-13	8.80	10.14	10.68	10.89	15.13	21.30	23.69

Table 22 - Incident wave heights ($H_{m0,IG,incident}$) and percent errors for the IG wave band for BC_702_IR_16_28 (TO5)

	WG	SB	NH	SWASH	% Error (SB)	% Error (NH)	% Error (SWASH)
WG-3	1.57	1.97	2.04	3.00	25.14	29.80	90.55
WG-6	2.54	2.60	2.55	3.29	2.35	0.40	29.68
WG-7	2.98	3.03	2.89	3.52	1.68	2.96	18.16
WG-8	3.34	3.26	3.08	3.64	2.38	7.89	8.90
WG-9	3.90	3.58	3.33	3.76	8.20	14.68	3.54
WG-10	4.14	3.75	3.43	3.76	9.24	17.05	9.09
WG-11	4.14	3.90	3.44	3.71	5.83	16.82	10.42
WG-12	3.97	4.12	3.43	3.56	3.83	13.57	10.38
WG-13	3.69	4.38	3.47	3.52	18.60	5.83	4.66

Table 23 - Incident wave heights ($H_{m0,SS,incident}$) and percent errors for the SS wave band for BC_702_IR_16_28 (TO5)

	WG	SB	NH	SWASH	% Error (SB)	% Error (NH)	% Error (SWASH)
WG-3	14.54	15.83	15.75	16.22	8.88	8.32	11.55
WG-6	15.17	16.61	16.29	16.93	9.53	7.43	11.62
WG-7	14.66	16.59	16.35	17.10	13.19	11.56	16.63
WG-8	14.51	16.29	16.23	16.98	12.25	11.85	17.01
WG-9	14.51	15.47	15.67	16.33	6.60	8.00	12.49
WG-10	13.91	14.57	14.87	15.43	4.68	6.89	10.87
WG-11	12.04	13.66	13.76	14.27	13.53	14.36	18.58
WG-12	9.49	11.87	11.63	12.06	25.12	22.60	27.15
WG-13	6.77	10.14	8.92	9.32	49.81	31.90	37.75

Appendix – B

R_708_IR_8_16

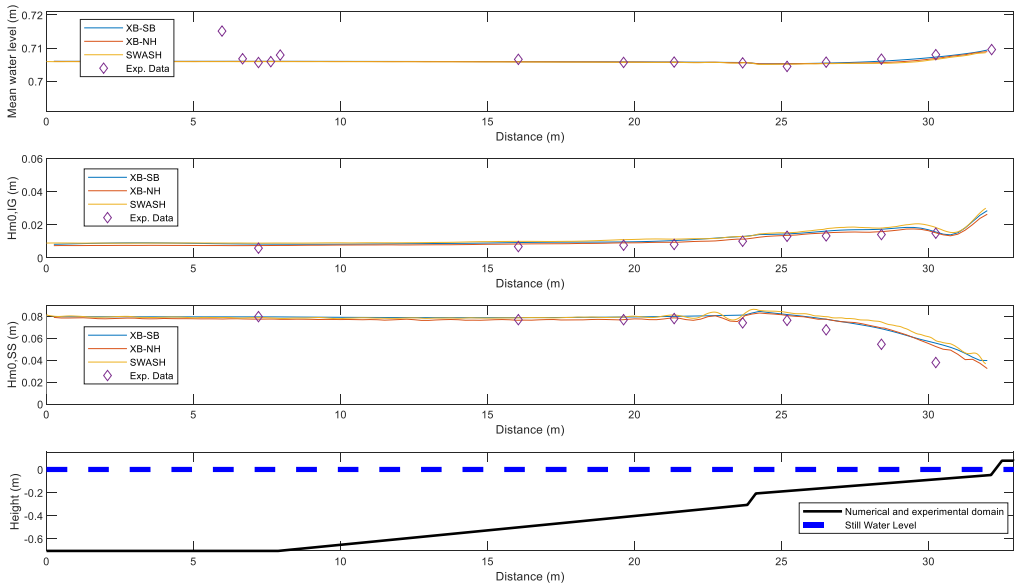

Figure 28 - Mean water depth (first panel) and total wave height for the infragravity (second panel) and sea-swell (third panel) waves along the domain for R_708_IR_8_16 (T06) for the three numerical (colored lines) and for the data (diamonds).

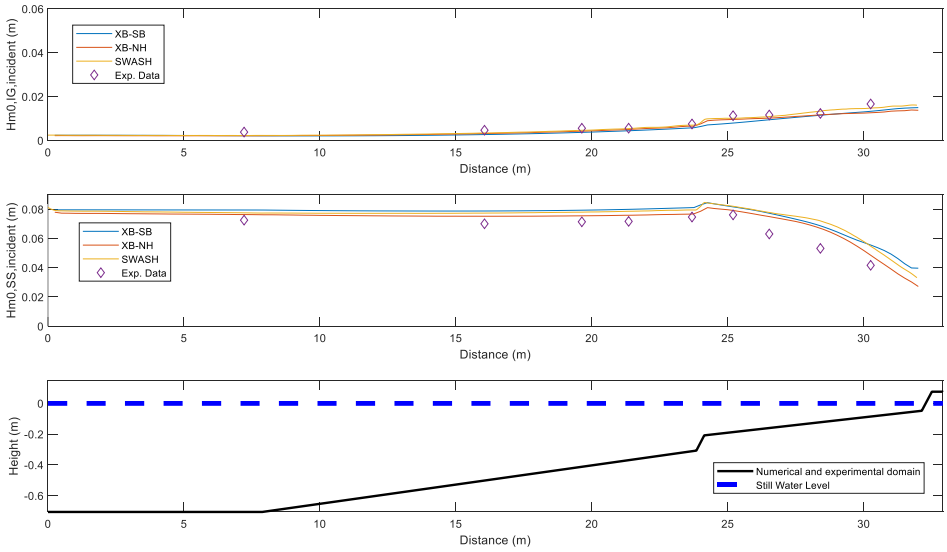

Figure 29 - Incident wave height for the infragravity (first panel) and sea-swell (second panel) waves along the domain for R_708_IR_8_16 (T06) for the three numerical (colored lines) and for the data (diamonds).

Table 24 – Total wave heights ($H_{m0,IG,total}$) and percent errors for the IG wave band for R_708_IR_8_16 (TO6)

	WG	SB	NH	SWASH	% Error (SB)	% Error (NH)	% Error (SWASH)
WG-3	0.59	0.83	0.74	0.89	42.22	26.72	51.96
WG-6	0.68	0.93	0.84	1.00	35.65	22.83	46.30
WG-7	0.76	0.96	0.91	1.10	26.30	18.91	44.32
WG-8	0.81	1.05	0.94	1.13	28.66	16.09	39.17
WG-9	1.00	1.29	1.13	1.30	28.84	12.93	29.12
WG-10	1.30	1.45	1.36	1.51	11.08	4.01	16.15
WG-11	1.33	1.62	1.51	1.77	21.80	13.60	33.13
WG-12	1.41	1.73	1.59	1.80	22.98	12.56	28.01
WG-13	1.49	1.56	1.51	1.83	5.03	1.71	23.17

Table 25 – Total wave heights ($H_{m0,SS,total}$) and percent errors for the SS wave band for R_708_IR_8_16 (TO6)

	WG	SB	NH	SWASH	% Error (SB)	% Error (NH)	% Error (SWASH)
WG-3	7.97	7.95	7.74	7.88	0.26	2.88	1.13
WG-6	7.69	7.88	7.64	7.86	2.43	0.69	2.22
WG-7	7.69	7.93	7.69	7.94	3.19	0.08	3.29
WG-8	7.79	7.99	7.86	8.12	2.56	0.84	4.19
WG-9	7.40	8.11	7.86	8.15	9.59	6.17	10.12
WG-10	7.63	8.16	8.08	8.35	6.96	5.82	9.38
WG-11	6.77	7.73	7.74	7.96	14.16	14.37	17.63
WG-12	5.45	6.87	6.94	7.48	25.99	27.39	37.27
WG-13	3.79	5.55	5.24	5.78	46.59	38.46	52.68

Table 26 – Incident wave heights ($H_{m0,IG,incident}$) and percent errors for the IG wave band for R_708_IR_8_16 (TO6)

	WG	SB	NH	SWASH	% Error (SB)	% Error (NH)	% Error (SWASH)
WG-3	0.38	0.22	0.21	0.23	43.40	44.06	40.93
WG-6	0.47	0.27	0.32	0.34	42.21	32.29	26.95
WG-7	0.56	0.37	0.43	0.47	33.57	23.81	16.62
WG-8	0.56	0.44	0.50	0.54	20.91	10.51	3.82
WG-9	0.75	0.58	0.65	0.70	23.27	13.39	6.97
WG-10	1.13	0.80	0.96	1.01	29.67	15.05	10.68
WG-11	1.16	0.95	1.02	1.10	18.63	12.11	5.75
WG-12	1.23	1.15	1.17	1.34	6.59	4.91	8.60
WG-13	1.67	1.33	1.26	1.48	20.10	24.09	11.38

Table 27 - Incident wave heights ($H_{m0,SS,incident}$) and percent errors for the SS wave band for R_708_IR_8_16 (T06)

	WG	SB	NH	SWASH	% Error (SB)	% Error (NH)	% Error (SWASH)
WG-3	7.25	7.95	7.64	7.75	9.58	5.28	6.91
WG-6	7.01	7.88	7.52	7.74	12.46	7.34	10.42
WG-7	7.14	7.93	7.55	7.80	11.13	5.75	9.26
WG-8	7.17	7.99	7.59	7.86	11.50	5.87	9.66
WG-9	7.47	8.11	7.67	7.95	8.62	2.73	6.48
WG-10	7.61	8.16	7.92	8.20	7.22	3.98	7.71
WG-11	6.31	7.73	7.50	7.77	22.47	18.83	23.17
WG-12	5.32	6.87	6.69	7.20	29.05	25.78	35.34
WG-13	4.16	5.55	4.85	5.47	33.30	16.55	31.41

R_708_IR_16_16

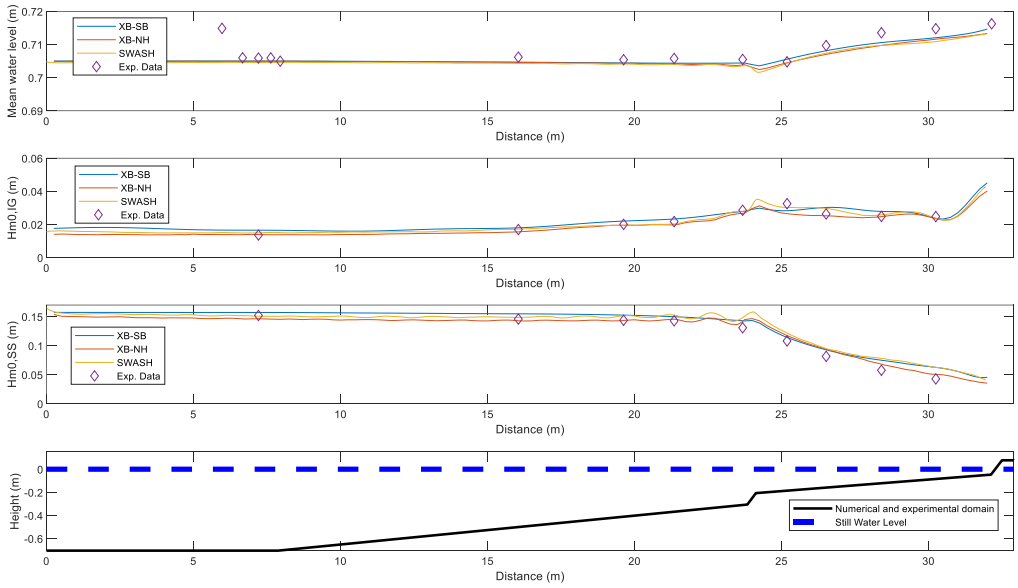

Figure 30 - Mean water depth (first panel) and total wave height for the infragravity (second panel) and sea-swell (third panel) waves along the domain for R_708_IR_16_16 (T07) for the three numerical (colored lines) and for the data (diamonds).

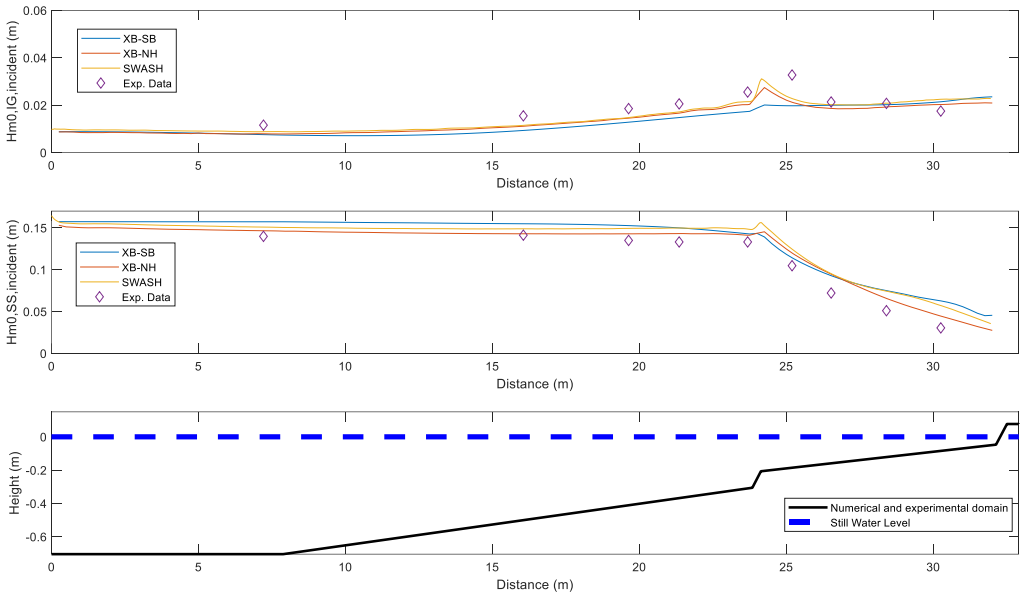

Figure 31 - Incident wave height for the infragravity (first panel) and sea-swell (second panel) waves along the domain for R_708_IR_16_16 (T07) for the three numerical (colored lines) and for the data (diamonds).

Table 28 - Total wave heights ($H_{m0,IG,total}$) and percent errors for the IG wave band for R_708_IR_16_16 (T07)

	WG	SB	NH	SWASH	% Error (SB)	% Error (NH)	% Error (SWASH)
WG-3	1.36	1.66	1.39	1.50	21.65	2.45	9.96
WG-6	1.69	1.80	1.56	1.72	6.19	8.11	1.68
WG-7	2.01	2.21	1.96	1.96	9.96	2.50	2.51
WG-8	2.18	2.33	1.98	2.03	7.19	8.98	6.67
WG-9	2.86	2.79	2.67	2.80	2.50	6.66	1.91
WG-10	3.26	2.83	2.65	3.02	13.10	18.52	7.14
WG-11	2.63	3.03	2.53	2.97	14.97	4.15	12.59
WG-12	2.49	2.79	2.47	2.59	12.11	0.47	4.10
WG-13	2.48	2.37	2.34	2.38	4.45	5.51	3.83

Table 29 – Total wave heights ($H_{m0,SS,total}$) and percent errors for the SS wave band for R_708_IR_16_16 (TO7)

	WG	SB	NH	SWASH	% Error (SB)	% Error (NH)	% Error (SWASH)
WG-3	15.20	15.72	14.65	15.07	3.43	3.66	0.90
WG-6	14.59	15.49	14.30	14.88	6.17	1.96	2.04
WG-7	14.38	15.27	14.35	15.16	6.17	0.22	5.43
WG-8	14.29	14.99	14.56	15.28	4.95	1.91	6.94
WG-9	13.09	14.29	14.16	14.90	9.21	8.21	13.89
WG-10	10.81	11.43	11.76	12.16	5.66	8.71	12.47
WG-11	8.16	9.29	9.42	9.46	13.73	15.32	15.90
WG-12	5.77	7.50	6.83	7.83	29.96	18.40	35.63
WG-13	4.28	6.27	5.06	6.27	46.42	18.11	46.21

Table 30 – Incident wave heights ($H_{m0,IG,incident}$) and percent errors for the IG wave band for R_708_IR_16_16 (TO7)

	WG	SB	NH	SWASH	% Error (SB)	% Error (NH)	% Error (SWASH)
WG-3	1.16	0.76	0.79	0.88	34.47	31.36	23.76
WG-6	1.55	0.94	1.11	1.15	39.69	28.29	25.90
WG-7	1.86	1.28	1.45	1.48	30.84	21.70	20.17
WG-8	2.06	1.48	1.67	1.72	28.03	18.96	16.48
WG-9	2.55	1.73	2.02	2.15	32.09	20.76	15.80
WG-10	3.27	1.98	2.12	2.28	39.62	35.09	30.45
WG-11	2.14	2.00	1.86	2.02	6.47	12.70	5.33
WG-12	2.08	2.02	1.92	2.08	2.67	7.34	0.43
WG-13	1.75	2.14	2.03	2.25	22.46	15.77	28.50

Table 31 - Incident wave heights ($H_{m0,SS,incident}$) and percent errors for the SS wave band for R_708_IR_16_16 (TO7)

	WG	SB	NH	SWASH	% Error (SB)	% Error (NH)	% Error (SWASH)
WG-3	13.98	15.72	14.65	15.09	12.46	4.79	7.92
WG-6	14.12	15.49	14.29	14.89	9.66	1.19	5.40
WG-7	13.50	15.27	14.29	14.94	13.11	5.84	10.66
WG-8	13.31	14.99	14.32	14.98	12.65	7.55	12.53
WG-9	13.31	14.29	14.11	14.84	7.35	6.02	11.47
WG-10	10.48	11.43	12.00	12.43	9.07	14.52	18.66
WG-11	7.21	9.29	9.46	9.48	28.76	31.23	31.42
WG-12	5.10	7.50	6.57	7.43	47.11	28.83	45.77
WG-13	3.04	6.27	4.46	5.71	106.07	46.33	87.69

R_708_IR_16_28

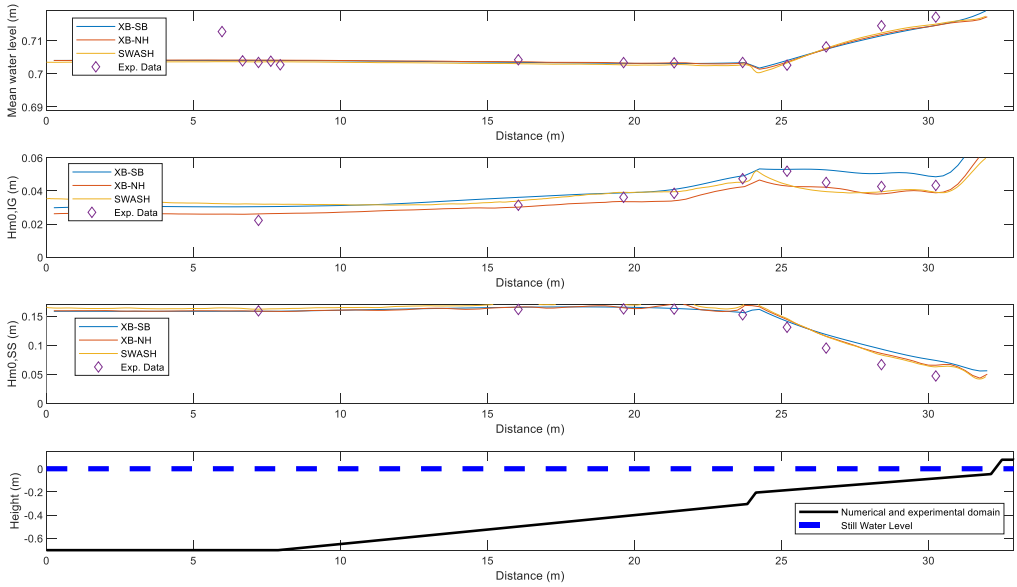

Figure 32 - Mean water depth (first panel) and total wave height for the infragravity (second panel) and sea-swell (third panel) waves along the domain for R_708_IR_16_28 (T08) for the three numerical (colored lines) and for the data (diamonds).

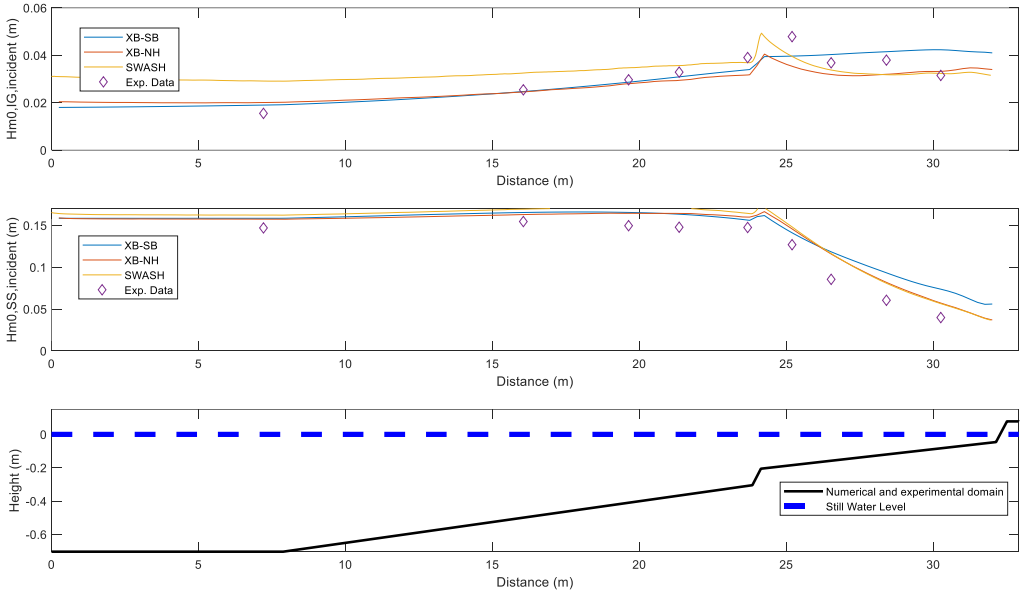

Figure 33 - Incident wave height for the infragravity (first panel) and sea-swell (second panel) waves along the domain for R_708_IR_16_28 (T08) for the three numerical (colored lines) and for the data (diamonds).

Table 32– Total wave heights ($H_{m0,IG,total}$) and percent errors for the IG wave band for R_708_IR_16_28 (TO8)

	WG	SB	NH	SWASH	% Error (SB)	% Error (NH)	% Error (SWASH)
WG-3	2.22	3.04	2.61	3.20	37.17	17.54	44.20
WG-6	3.13	3.61	3.02	3.39	15.19	3.68	8.24
WG-7	3.61	3.88	3.35	3.91	7.32	7.22	8.23
WG-8	3.85	4.09	3.40	3.95	6.18	11.65	2.56
WG-9	4.73	4.91	4.24	4.53	3.69	10.36	4.35
WG-10	5.18	5.30	4.30	4.38	2.19	17.13	15.60
WG-11	4.50	5.27	4.22	3.95	16.89	6.36	12.29
WG-12	4.26	5.06	3.82	3.95	18.54	10.42	7.41
WG-13	4.33	4.85	3.88	3.92	12.00	10.31	9.52

Table 33 – Total wave heights ($H_{m0,SS,total}$) and percent errors for the SS wave band for R_708_IR_16_28 (TO8)

	WG	SB	NH	SWASH	% Error (SB)	% Error (NH)	% Error (SWASH)
WG-3	15.92	15.85	15.85	16.21	0.45	0.40	1.84
WG-6	16.16	16.54	16.57	17.10	2.32	2.53	5.78
WG-7	16.25	16.54	16.44	17.03	1.81	1.17	4.80
WG-8	16.21	16.33	17.05	17.55	0.75	5.18	8.26
WG-9	15.24	15.63	16.57	16.93	2.59	8.77	11.09
WG-10	13.09	14.11	14.43	14.57	7.81	10.23	11.32
WG-11	9.51	11.84	11.54	11.45	24.56	21.37	20.40
WG-12	6.66	9.33	8.58	8.33	40.13	28.87	25.05
WG-13	4.71	7.38	6.56	6.27	56.77	39.35	33.33

Table 34 – Incident wave heights ($H_{m0,IG,incident}$) and percent errors for the IG wave band for R_708_IR_16_28 (TO8)

	WG	SB	NH	SWASH	% Error (SB)	% Error (NH)	% Error (SWASH)
WG-3	1.55	1.90	2.01	2.91	22.62	29.57	87.97
WG-6	2.54	2.47	2.45	3.25	2.82	3.49	27.86
WG-7	2.97	2.87	2.80	3.48	3.40	5.55	17.16
WG-8	3.29	3.09	2.94	3.57	6.03	10.49	8.45
WG-9	3.90	3.39	3.17	3.69	13.15	18.80	5.48
WG-10	4.79	3.97	3.54	3.95	17.15	26.07	17.52
WG-11	3.68	4.03	3.19	3.37	9.44	13.35	8.44
WG-12	3.80	4.15	3.20	3.18	9.34	15.72	16.21
WG-13	3.15	4.23	3.32	3.24	34.35	5.34	2.68

Table 35 - Incident wave heights ($H_{m0,SS,incident}$) and percent errors for the SS wave band for R_708_IR_16_28 (TO8)

	WG	SB	NH	SWASH	% Error (SB)	% Error (NH)	% Error (SWASH)
WG-3	14.69	15.85	15.74	16.23	7.83	7.13	10.44
WG-6	15.46	16.54	16.29	16.93	7.00	5.41	9.57
WG-7	14.96	16.54	16.44	17.10	10.60	9.89	14.32
WG-8	14.78	16.33	16.42	17.04	10.52	11.13	15.27
WG-9	14.75	15.63	15.99	16.43	5.99	8.43	11.38
WG-10	12.69	14.11	14.58	14.80	11.21	14.86	16.58
WG-11	8.55	11.84	11.58	11.57	38.47	35.39	35.30
WG-12	6.05	9.33	8.19	8.08	54.26	35.39	33.62
WG-13	3.98	7.38	5.72	5.65	85.14	43.47	41.71

Appendix – C

K_708_IR_8_16

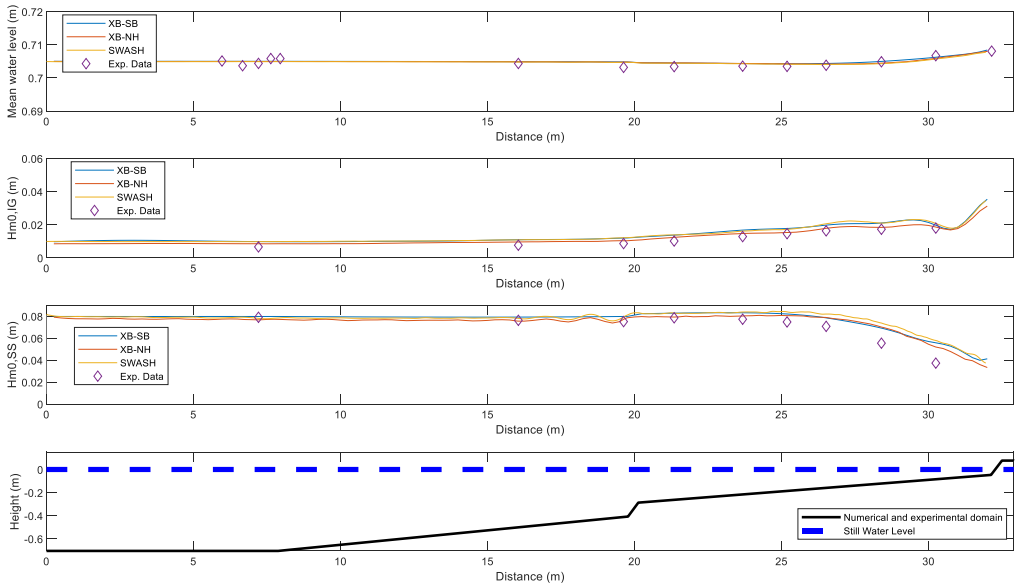

Figure 34 - Mean water depth (first panel) and total wave height for the infragravity (second panel) and sea-swell (third panel) waves along the domain for K_708_IR_8_16 (T09) for the three numerical (colored lines) and for the data (diamonds).

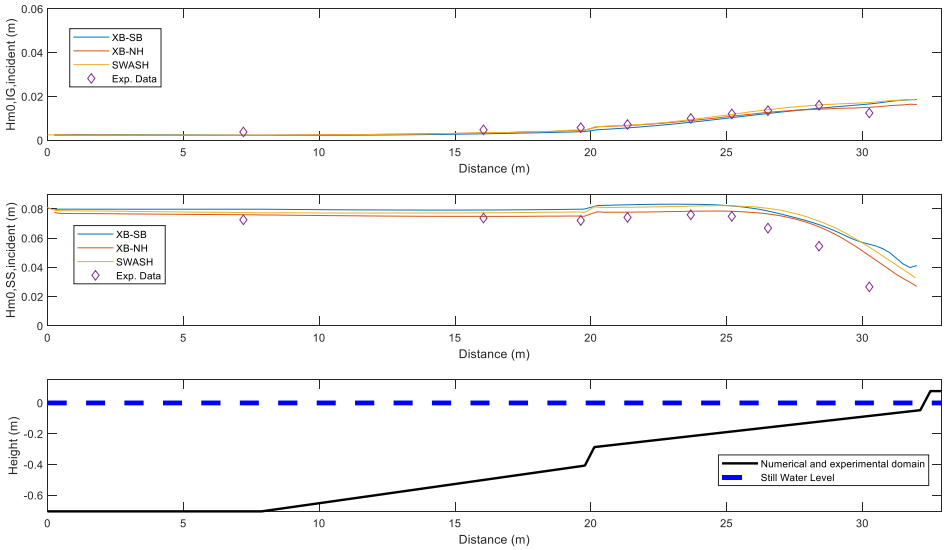

Figure 35 - Incident wave height for the infragravity (first panel) and sea-swell (second panel) waves along the domain for K_708_IR_8_16 (T09) for the three numerical (colored lines) and for the data (diamonds).

Table 36 - Total wave heights ($H_{m0,IG,total}$) and percent errors for the IG wave band for K_708_IR_8_16 (TO9)

	WG	SB	NH	SWASH	% Error (SB)	% Error (NH)	% Error (SWASH)
WG-3	0.66	0.98	0.85	0.98	48.63	28.89	48.34
WG-6	0.76	1.10	0.96	1.09	43.55	25.86	42.38
WG-7	0.86	1.20	1.03	1.22	38.62	19.73	40.63
WG-8	1.02	1.38	1.24	1.39	35.33	21.73	36.39
WG-9	1.28	1.68	1.47	1.62	30.53	14.67	25.82
WG-10	1.46	1.78	1.53	1.73	21.44	4.74	17.98
WG-11	1.63	1.98	1.78	2.07	21.14	9.27	26.75
WG-12	1.73	2.11	1.84	2.10	21.83	6.42	21.50
WG-13	1.80	1.97	1.86	2.08	9.75	3.61	15.67

Table 37 - Total wave heights ($H_{m0,SS,total}$) and percent errors for the SS wave band for K_708_IR_8_16 (TO9)

	WG	SB	NH	SWASH	% Error (SB)	% Error (NH)	% Error (SWASH)
WG-3	7.91	7.98	7.68	7.81	0.92	2.94	1.23
WG-6	7.63	7.93	7.56	7.81	3.85	1.00	2.28
WG-7	7.52	7.99	7.73	7.97	6.24	2.84	6.09
WG-8	7.86	8.29	7.93	8.30	5.39	0.89	5.52
WG-9	7.73	8.32	8.03	8.39	7.62	3.82	8.54
WG-10	7.48	8.21	8.06	8.40	9.72	7.68	12.27
WG-11	7.08	7.86	7.89	8.20	10.95	11.42	15.84
WG-12	5.55	6.92	7.02	7.39	24.77	26.45	33.09
WG-13	3.73	5.59	5.20	5.80	49.68	39.36	55.39

Table 38 - Incident wave heights ($H_{m0,IG,incident}$) and percent errors for the IG wave band for K_708_IR_8_16 (TO9)

	WG	SB	NH	SWASH	% Error (SB)	% Error (NH)	% Error (SWASH)
WG-3	0.38	0.23	0.23	0.23	39.49	40.37	39.02
WG-6	0.48	0.30	0.34	0.34	37.67	28.18	27.81
WG-7	0.58	0.39	0.45	0.46	31.83	21.28	19.58
WG-8	0.72	0.57	0.68	0.68	21.39	6.31	5.51
WG-9	1.00	0.82	0.90	0.95	17.43	9.75	4.69
WG-10	1.20	1.03	1.10	1.18	14.01	8.24	1.62
WG-11	1.35	1.22	1.27	1.40	9.59	5.91	3.41
WG-12	1.60	1.46	1.42	1.61	8.56	11.10	0.80
WG-13	1.25	1.66	1.51	1.73	33.08	21.00	38.46

Table 39 - Incident wave heights ($H_{m0,SS,incident}$) and percent errors for the SS wave band for K_708_IR_8_16 (T09)

	WG	SB	NH	SWASH	% Error (SB)	% Error (NH)	% Error (SWASH)
WG-3	7.26	7.98	7.60	7.75	10.02	4.80	6.83
WG-6	7.38	7.93	7.49	7.74	7.48	1.55	4.89
WG-7	7.21	7.99	7.52	7.79	10.74	4.26	7.96
WG-8	7.42	8.29	7.78	8.12	11.61	4.79	9.35
WG-9	7.60	8.32	7.84	8.20	9.42	3.14	7.79
WG-10	7.49	8.21	7.84	8.21	9.55	4.59	9.54
WG-11	6.69	7.86	7.66	8.04	17.49	14.53	20.17
WG-12	5.45	6.92	6.77	7.17	26.98	24.24	31.41
WG-13	2.67	5.59	4.81	5.39	109.32	80.13	101.90

K_708_IR_16_16

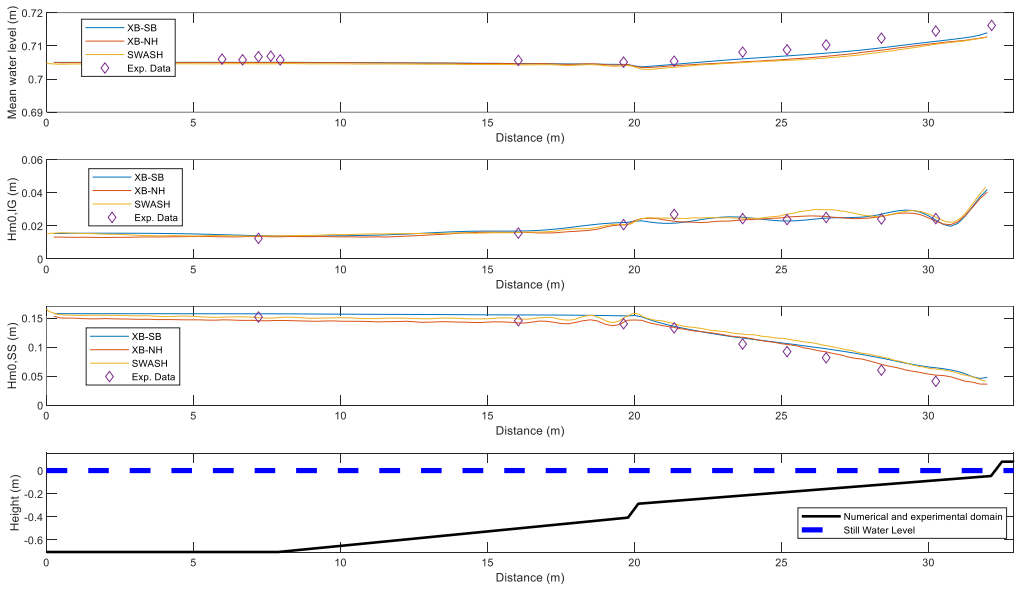

Figure 36 - Mean water depth (first panel) and total wave height for the infragravity (second panel) and sea-swell (third panel) waves along the domain for K_708_IR_16_16 (T10) for the three numerical (colored lines) and for the data (diamonds).

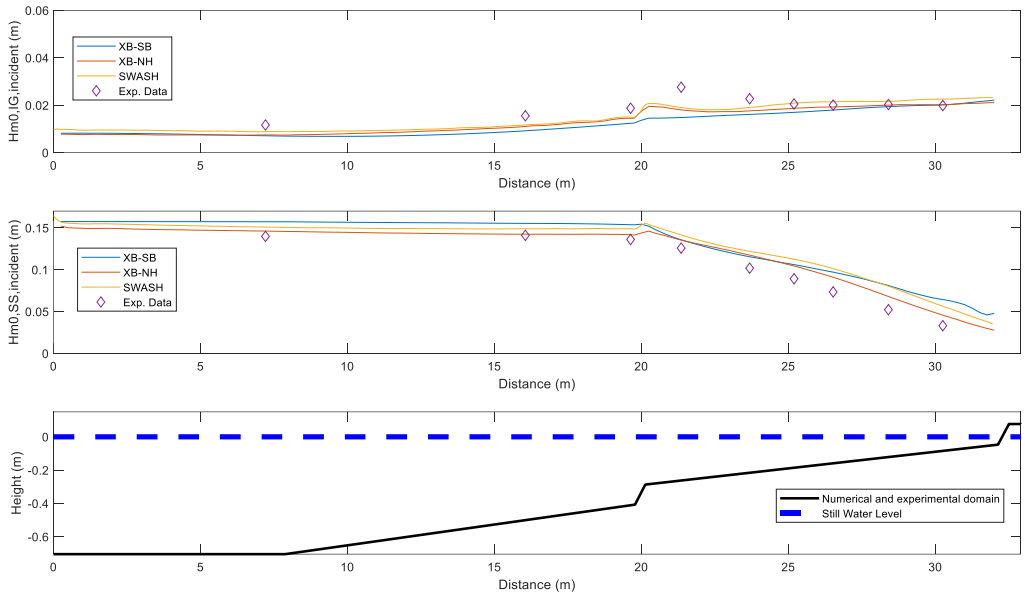

Figure 37- Incident wave height for the infragravity (first panel) and sea-swell (second panel) waves along the domain for K_708_IR_16_16 (T10) for the three numerical (colored lines) and for the data (diamonds).

Table 40 – Total wave heights ($H_{m0,IG,total}$) and percent errors for the IG wave band for K_708_IR_16_16 (T10)

	WG	SB	NH	SWASH	% Error (SB)	% Error (NH)	% Error (SWASH)
WG-3	1.24	1.41	1.36	1.39	13.04	9.08	11.81
WG-6	1.56	1.69	1.60	1.60	7.90	2.63	2.60
WG-7	2.07	2.20	2.06	2.06	6.12	0.77	0.53
WG-8	2.69	2.16	2.27	2.46	19.64	15.50	8.59
WG-9	2.43	2.52	2.36	2.46	3.55	3.08	1.31
WG-10	2.38	2.29	2.53	2.71	3.75	6.45	13.69
WG-11	2.50	2.46	2.57	2.97	1.58	2.50	18.84
WG-12	2.41	2.71	2.57	2.59	12.14	6.35	7.53
WG-13	2.44	2.35	2.28	2.52	3.76	6.29	3.36

Table 41 - Total wave heights ($H_{m0,SS,total}$) and percent errors for the SS wave band for K_708_IR_16_16 (T10)

	WG	SB	NH	SWASH	% Error (SB)	% Error (NH)	% Error (SWASH)
WG-3	15.17	15.73	14.55	15.07	3.68	4.07	0.64
WG-6	14.54	15.53	14.16	14.83	6.85	2.60	2.05
WG-7	14.01	15.37	14.28	15.04	9.71	1.92	7.36
WG-8	13.31	13.57	13.37	14.05	1.97	0.48	5.53
WG-9	10.52	11.55	11.69	12.21	9.76	11.08	16.07
WG-10	9.22	10.60	10.45	11.38	15.01	13.36	23.44
WG-11	8.16	9.71	9.18	10.23	18.96	12.46	25.39
WG-12	6.02	8.11	7.03	8.33	34.59	16.71	38.24
WG-13	4.11	6.43	5.17	6.23	56.69	26.01	51.67

Table 42 - Incident wave heights ($H_{m0,IG,incident}$) and percent errors for the IG wave band for K_708_IR_16_16 (T10)

	WG	SB	NH	SWASH	% Error (SB)	% Error (NH)	% Error (SWASH)
WG-3	1.16	0.71	0.75	0.88	38.95	35.86	24.21
WG-6	1.55	0.92	1.10	1.17	40.76	28.98	24.78
WG-7	1.87	1.24	1.45	1.49	33.96	22.63	20.50
WG-8	2.76	1.48	1.80	1.90	46.34	34.67	31.13
WG-9	2.27	1.61	1.76	1.91	29.10	22.48	15.99
WG-10	2.05	1.70	1.87	2.09	17.16	8.63	1.91
WG-11	2.01	1.80	1.92	2.15	10.49	4.11	7.03
WG-12	2.03	1.94	2.00	2.17	4.30	1.23	6.85
WG-13	1.98	2.01	2.02	2.26	1.55	1.61	13.81

Table 43 - Incident wave heights ($H_{m0,SS,incident}$) and percent errors for the SS wave band for K_708_IR_16_16 (T10)

	WG	SB	NH	SWASH	% Error (SB)	% Error (NH)	% Error (SWASH)
WG-3	13.98	15.73	14.61	15.09	12.50	4.53	7.96
WG-6	14.10	15.53	14.24	14.88	10.15	0.98	5.53
WG-7	13.61	15.37	14.19	14.88	13.00	4.30	9.39
WG-8	12.58	13.57	13.54	14.16	7.91	7.62	12.55
WG-9	10.18	11.55	11.74	12.18	13.39	15.28	19.62
WG-10	8.92	10.60	10.44	11.25	18.88	17.02	26.12
WG-11	7.34	9.71	9.09	10.10	32.20	23.81	37.49
WG-12	5.22	8.11	6.80	8.02	55.29	30.23	53.63
WG-13	3.31	6.43	4.57	5.63	94.55	38.08	70.23

K_708_IR_16_28

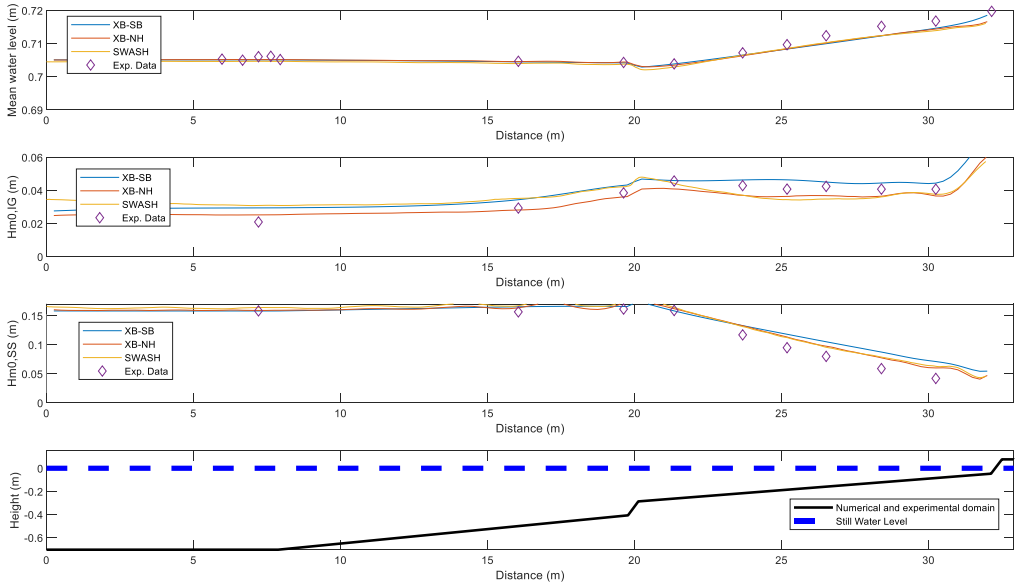

Figure 38 - Mean water depth (first panel) and total wave height for the infragravity (second panel) and sea-swell (third panel) waves along the domain for K_708_IR_16_28 (T11) for the three numerical (colored lines) and for the data (diamonds).

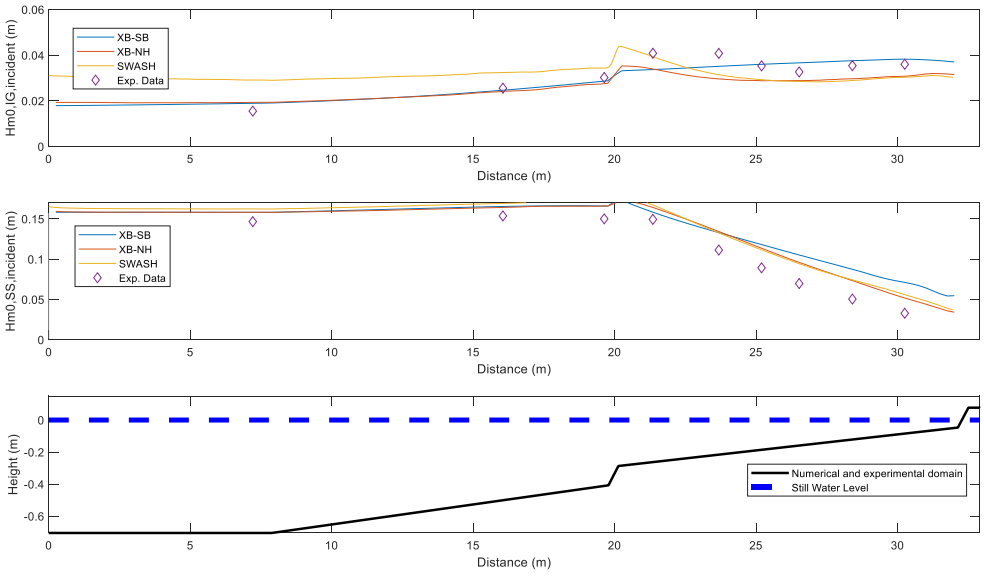

Figure 39 - Incident wave height for the infragravity (first panel) and sea-swell (second panel) waves along the domain for K_708_IR_16_28 (T11) for the three numerical (colored lines) and for the data (diamonds).

Table 44 - Total wave heights ($H_{m0,IG,total}$) and percent errors for the IG wave band for K_708_IR_16_28 (T11)

	WG (cm)	SB (cm)	NH (cm)	SWASH (cm)	% Error (SB)	% Error (NH)	% Error (SWASH)
WG-3	2.09	2.94	2.52	3.09	40.62	20.49	47.61
WG-6	2.93	3.44	2.82	3.52	17.21	3.93	19.85
WG-7	3.85	4.30	3.62	4.22	11.85	6.04	9.63
WG-8	4.57	4.59	4.09	4.43	0.61	10.52	3.02
WG-9	4.29	4.63	3.70	3.70	7.97	13.69	13.63
WG-10	4.08	4.64	3.64	3.44	13.76	10.78	15.61
WG-11	4.24	4.50	3.68	3.48	6.13	13.21	18.03
WG-12	4.07	4.45	3.65	3.61	9.16	10.42	11.39
WG-13	4.07	4.44	3.66	3.76	9.07	10.01	7.51

Table 45 – Total wave heights ($H_{m0,SS,total}$) and percent errors for the SS wave band for K_708_IR_16_28 (T11)

	WG (cm)	SB (cm)	NH (cm)	SWASH (cm)	% Error (SB)	% Error (NH)	% Error (SWASH)
WG-3	15.83	15.82	15.91	16.40	0.10	0.49	3.59
WG-6	15.66	16.54	16.35	16.72	5.62	4.42	6.80
WG-7	16.14	16.59	17.37	17.62	2.79	7.61	9.18
WG-8	15.90	15.83	16.20	16.42	0.48	1.89	3.27
WG-9	11.70	13.29	13.28	13.11	13.58	13.51	12.07
WG-10	9.50	11.81	11.34	11.22	24.37	19.42	18.19
WG-11	8.00	10.52	9.75	9.54	31.44	21.91	19.18
WG-12	5.89	8.74	7.75	7.88	48.35	31.46	33.72
WG-13	4.20	7.12	6.01	6.29	69.26	43.00	49.60

Table 46 – Incident wave heights ($H_{m0,IG,incident}$) and percent errors for IG wave band for K_708_IR_16_28 (T11)

	WG (cm)	SB (cm)	NH (cm)	SWASH (cm)	% Error (SB)	% Error (NH)	% Error (SWASH)
WG-3	1.55	1.89	1.93	2.91	22.21	24.70	88.06
WG-6	2.55	2.46	2.41	3.24	3.50	5.56	26.76
WG-7	3.02	2.86	2.75	3.44	5.30	8.86	13.73
WG-8	4.08	3.37	3.39	3.94	17.45	16.88	3.54
WG-9	4.08	3.51	2.96	3.14	13.87	27.39	22.95
WG-10	3.53	3.60	2.88	2.92	1.92	18.42	17.19
WG-11	3.26	3.66	2.88	2.85	12.26	11.66	12.78
WG-12	3.54	3.76	2.97	2.89	6.16	16.22	18.28
WG-13	3.60	3.82	3.07	3.03	6.17	14.63	15.84

Table 47 – Incident wave heights ($H_{m0,SS,incident}$) and percent errors for the SS wave band for K_708_IR_16_16 (T11)

	WG (cm)	SB (cm)	NH (cm)	SWASH (cm)	% Error (SB)	% Error (NH)	% Error (SWASH)
WG-3	14.66	15.82	15.82	16.24	7.93	7.91	10.78
WG-6	15.37	16.54	16.42	16.91	7.64	6.84	10.08
WG-7	15.00	16.59	16.61	17.06	10.60	10.76	13.76
WG-8	14.93	15.83	16.42	16.71	5.98	9.91	11.91
WG-9	11.13	13.29	13.44	13.23	19.41	20.72	18.89
WG-10	8.92	11.81	11.36	11.15	32.32	27.32	24.99
WG-11	6.97	10.52	9.60	9.40	50.87	37.74	34.82
WG-12	5.04	8.74	7.33	7.43	73.34	45.37	47.38
WG-13	3.29	7.12	5.17	5.59	116.55	57.48	70.25